

Active Quantum Reservoir Engineering: Using a Qubit to Manipulate its Environment

Marcelo Janovitch¹, Matteo Brunelli^{2,1}, and Patrick P. Potts¹

¹Department of Physics and Swiss Nanoscience Institute, University of Basel, Klingelbergstrasse 82, 4056 Basel, Switzerland

²JEIP, UAR 3573 CNRS, Collège de France, PSL Research University, 11 Place Marcelin Berthelot, 75321 Paris Cedex 05, France

Quantum reservoir engineering leverages dissipative processes to achieve desired behavior, with applications ranging from entanglement generation to quantum error correction. Therein, a structured environment acts as an entropy sink for the system, and no time-dependent control over the system is required. We develop a theoretical framework for *active* reservoir engineering, where time-dependent control over a quantum system is used to manipulate its environment. In this case, the system may act as an entropy sink for the environment. Our framework captures the dynamical interplay between system and environment, and provides an intuitive picture of how finite-size effects and system-environment correlations allow for manipulating the environment by repeated initialization of the quantum system. We illustrate our results with two examples: a superconducting qubit coupled to an environment of two-level systems and a semiconducting quantum dot coupled to nuclear spins. In both scenarios, we find qualitative agreement with previous experimental results, illustrating how active control can unlock new functionalities in open quantum systems.

1 Introduction

Quantum systems inevitably couple to their surroundings. This is the virtue that allows them to be observed and the chagrin that ruins their unique quantum properties. To minimize unwanted noise and decoherence, they are typically

kept as isolated from their environment as possible. In recent decades, dissipative processes have been recognized not only as a source of decoherence but also as a resource. This insight underpins quantum reservoir engineering [1–3], where controlled dissipation enables desired functionality, such as non-reciprocity [4], topology [5] and autonomous quantum error correction [6–9], or stabilizes resourceful states such as entangled [10–15] or squeezed states [16–18]. A key ingredient in reservoir engineering is a low-entropy environment, typically the vacuum state of the electromagnetic field.

In many scenarios of interest, a low-entropy environment is not available because the relevant energy scales are comparable to temperature, rendering the standard approach to reservoir engineering inapplicable. This is typically the case in solid state qubits; the collective magnetization of the material hosting the qubit can act as a bath, composed, e.g., of nuclear spins for spin qubits [19] or two-level defects for superconducting qubits [20–22]. In this case, time-dependent control over the quantum system opens the door to a novel, *active* approach to reservoir engineering, where the environment is manipulated through the system. Once the environment state is tailored, it can add functionality to the quantum system, acting as an engineered dissipative channel.

Active reservoir engineering protocols have already been experimentally implemented. For instance, it has been shown that repeated resetting of a superconducting qubit to the ground state allows for cooling of the environment [21]. Furthermore, spin qubits in semiconductors have been extensively used to manipulate the magnetization of their surrounding nuclei, also known as dynamic nuclear polarization [19]; this led

Marcelo Janovitch: m.janovitch@unibas.ch

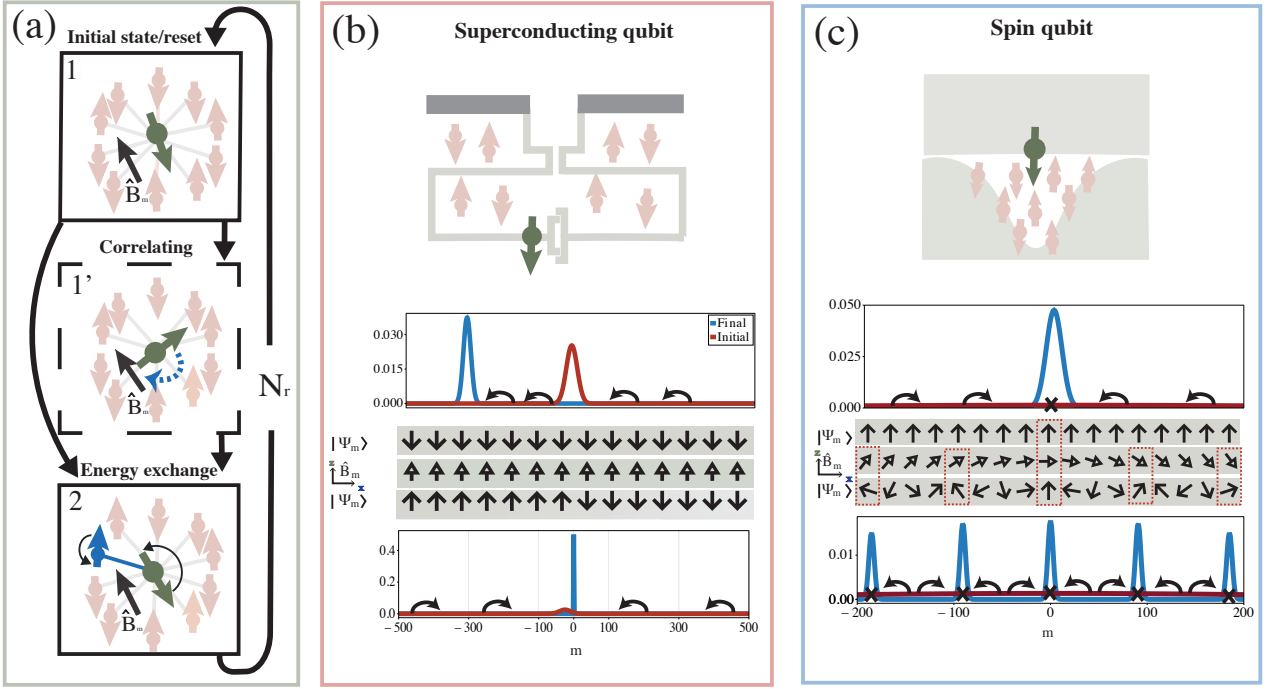


Figure 1: Actively engineering the environment of a qubit. (a) Cyclic operation implementing active reservoir engineering. After initializing the qubit (step 1), it may be correlated with the environment (step 1') before exchanging energy (step 2). These steps are repeated multiple times to manipulate the magnetization of the environment. (b) Active reservoir engineering using a superconducting qubit. Probability of the reservoir's magnetization before (red) and after (blue) active reservoir engineering are shown for two different protocols, together with the Bloch vectors for the state after initialization (arrows with open heads) and the direction of the magnetic field \vec{B}_m (arrows with closed heads). Whenever the Bloch vector points in the same (opposite) direction as \vec{B}_m , the magnetization increases (decreases), as illustrated by the curved arrows. The middle panel shows how repeated preparation of the state $|\downarrow_z\rangle$ results in cooling of the environment. The bottom illustrates how a correlated state can be used for cooling the environment if it has positive m and heating it for negative m , resulting in a narrowing of the magnetization. (c) Active reservoir engineering using a spin qubit. The middle illustrates how repeatedly preparing the state $|\uparrow_z\rangle$ results in narrowing of the magnetization, because the field \vec{B}_m rotates. The bottom shows how a correlated state can be used to create periodic narrowing, resulting in a distribution with multiple peaks. Dotted red boxes denote attractors of the magnetization, where the state's Bloch vector is perpendicular to the field. Here $\Delta = 0$. For the superconducting qubit, we consider $N_r = 10^3$ iterations, and for the spin qubit $N_r = 10^6$.

to orders of magnitude improvement in coherence time [23–28]. Compared to conventional (or passive) reservoir engineering, where the environment acts as an entropy sink and no time-dependent control over the system is required, the roles of system and environment are exchanged in active reservoir engineering: the system acts as an entropy sink for the environment. Despite its potential, a theoretical framework for active reservoir engineering remains largely undeveloped.

In this work, we fill this gap by deriving and analyzing a theoretical framework for active reservoir engineering. This framework allows for an intuitive understanding of the joint system-bath dynamics and provides results that are in

qualitative agreement with existing experiments. It provides, to the best of our knowledge, the only tractable framework that captures finite-size effects and strong classical system-bath correlations, offering efficient simulations and analytic solutions where fully quantum methods are seldom tractable. While we focus on specific platforms, our results apply to different central spin systems, including NV-centers [29, 30] and we provide general derivations which can be used to treat systems beyond qubits.

2 Overview

To illustrate our framework that is detailed in Sec. 3, we focus on the two scenarios sketched in

Fig 1, a superconducting qubit coupled to a bath of two-level systems, motivated by the experiment in Ref. [21], and a semiconducting quantum dot coupled to nuclear spins, motivated by Refs. [27, 28, 31]. In both cases, we consider a protocol where repeated initialization of the system (henceforth called qubit) allows for manipulating the magnetization, m , of the environment by altering its probability distribution P_m . For a given magnetization, the qubit will precess around an effective magnetic field \vec{B}_m , which depends on m . In addition, the qubit may exchange energy with the environment. This occurs through incoherent flip-flop processes, where the qubit and an environmental spin (or two-level system) flip together. Importantly, these processes are also dependent on the effective field \vec{B}_m . The Bloch vector of the qubit flips from being parallel to antiparallel with the magnetic field, or vice versa. If the qubit starts out (anti-)parallel to \vec{B}_m , then the flip-flop process increases (decreases) the magnetization m by one, c.f. Fig. 1 (a). This provides an intuitive understanding of different strategies for active reservoir engineering: if the magnetization should decrease, the qubit should be prepared with a Bloch vector that points in the direction opposite to \vec{B}_m . To increase the magnetization, a state parallel to \vec{B}_m should be prepared.

2.1 Superconducting qubit

For the superconducting qubit, we consider an environment of two-level systems (TLSs) that have approximately the same splitting as the qubit itself, such that energy exchanges between the system and environment are almost resonant. In this scenario, the effective field \vec{B}_m is particularly simple — it always points in the positive z -direction, see Fig. 1 (b). The magnetization of the environment can thus be decreased by initializing the system in the spin-down state $|\downarrow_z\rangle$. Repeatedly initializing this state results in the environment being cooled, as it moves to lower energy states, see Fig. 1. This protocol was employed in the experiment of Ref. [21]. Conversely, repeated initialization in the spin-up state $|\uparrow_z\rangle$, results in population inversion (increased magnetization) as also demonstrated experimentally in Ref. [21].

Refined control of the state of the environment is possible by exploiting correlations between the

system and the environment. As a simple example, consider the state $|\downarrow_z\rangle$ for $m > 0$ and $|\uparrow_z\rangle$ for $m < 0$. In this case, the magnetization is decreased for positive m and increased for negative m , resulting in a concentration of population in the $m = 0$ state, as illustrated in Fig. 1 (b). While this correlated state may be difficult to prepare, it illustrates the potential of exploiting correlations to manipulate the state of the environment.

The superconducting qubit scenario, together with the protocols introduced here, is discussed in detail in Sec. 4.

2.2 Quantum dot spin qubit

In the quantum dot spin qubit scenario, there is a large mismatch between the energy splitting of the qubit and the nuclear spins that constitute the environment [27, 28, 32]. To enable energy transfer between the system and the environment, a Rabi drive with strength Ω is applied close to resonance with the nuclei frequencies (Hartmann-Hahn resonance). This has two important consequences. First, the energy exchange between the system and the environment can be switched off by removing the Rabi drive. Second, the direction of the field $\vec{B}_m = (\Delta - m|A_c|)\hat{e}_z + \Omega\hat{e}_x$ depends on the magnetization of the environment as illustrated in Fig. 1 c). Here Δ is the detuning of the drive and A_c is a coupling strength. For large positive (negative) magnetization, the field points down (up) in the z -direction. In between it rotates, pointing in the x -direction at $m|A_c| = \Delta$. This m -dependence of the field direction implies that if we repeatedly prepare the state $|\uparrow_z\rangle$, the magnetization will decrease (increase) for large positive (negative) m , resulting in a concentration of population around $m = 0$. This protocol has been implemented experimentally in Refs. [28, 31], increasing the decoherence time of the spin qubit by one order of magnitude.

As for the superconducting qubit, further control of the bath is enabled by exploiting correlations. In the quantum dot spin qubit, a way to create such correlations is to switch off the Rabi drive and use the free evolution in the m -dependent field in a Ramsey protocol. In this manner, a state can be prepared with a Bloch vector that rotates in the xz -plane as a function of m , see Fig. 1 c). This state will result in peri-

odic increase and decrease of the magnetization as a function of m , creating peaks in its distribution by repeated preparation. A distribution with such qualitative features was observed experimentally in Ref. [27]. Furthermore, as the locations of the peaks depend on the duration of the Ramsey protocol, all peaks except the one at $m = 0$ can be suppressed by changing this duration from preparation to preparation. This protocol was implemented in Refs. [27, 28, 31], increasing the coherence time by two orders of magnitude.

The quantum dot spin qubit scenario and the protocols discussed here are presented in more detail in Sec. 5.

3 Master equation for active reservoir engineering

To describe active reservoir engineering protocols, we derive a master equation that keeps track not only of the system, but also the observable of interest in the environment. This is achieved through the technique of correlated projectors [33–39]. In App. A we provide detailed derivation for an arbitrary quantum system. In contrast to Refs. [38, 39] we treat part of the system-environment interaction non-perturbatively, leading to a more general master

equation with qualitatively different features.

We focus on central spin models described by the Hamiltonian,

$$H = \vec{B}_0 \cdot \vec{S} + \sum_{k=1}^N \omega_k I_z^k + \sum_{k=1}^N \vec{S} \mathbf{A} \vec{I}_k, \quad (1)$$

where $\vec{S} = (S_x, S_y, S_z)$ are spin-1/2 operators describing the system qubit, $\vec{I}_k = (I_x^k, I_y^k, I_z^k)$ are spin- s operators describing the environment, ω_k the frequencies of each bath constituent, and \mathbf{A} is a 3×3 coupling matrix describing an anisotropic hyperfine contact interaction. For simplicity, we consider that each spin in the environment couples identically to the system. Inhomogeneous couplings are considered in App. B, where we specialise the MARE to a large class of central spin systems. We note that Eq. (1) is beyond the integrable Gaudin magnets, due to the anisotropy in the coupling [37, 40–44] —the full quantum mechanical treatment of the bath thus typically relies on costly numeric simulations [45–47].

The MARE derived from Eq. (1) provides the joint dynamics for the qubit and the magnetization of the environment, which is defined as the eigenvalue of the collective spin operator $J_z = \sum_k I_z^k$. The joint state of the qubit and the magnetization is denoted $\rho_m(t)$. The system density matrix can be obtained via $\rho_S(t) = \sum_m \rho_m(t)$ and the probability distribution of the magnetization through $\text{tr } \rho_m = P_m$. The MARE reads

$$\begin{aligned} \partial_t \rho_m = & -i [\vec{B}_m \cdot \vec{S}, \rho_m] + \Gamma_m \left[|\downarrow_m\rangle\langle\uparrow_{m-1}| \frac{\rho_{m-1}}{V_{m-1}} |\uparrow_{m-1}\rangle\langle\downarrow_m| - \frac{1}{2} \left\{ |\downarrow_m\rangle\langle\downarrow_m|, \frac{\rho_m}{V_m} \right\} \right] \\ & + \Gamma_{m+1} \left[|\uparrow_m\rangle\langle\downarrow_{m+1}| \frac{\rho_{m+1}}{V_{m+1}} |\downarrow_{m+1}\rangle\langle\uparrow_m| - \frac{1}{2} \left\{ |\uparrow_m\rangle\langle\uparrow_m|, \frac{\rho_m}{V_m} \right\} \right], \end{aligned} \quad (2)$$

where the state $|\uparrow_m\rangle$ ($|\downarrow_m\rangle$) corresponds to a Bloch vector that points in the same (opposite) direction as \vec{B}_m . The volume factors, V_m , give the number of states with a given magnetization (i.e., the number of eigenstates of J_z with eigenvalue m). Our MARE has the general form shown in Ref. [36] to describe non-Markovian dynamics of ρ_S .

The first term in Eq. (2) corresponds to the unitary rotation of the qubit around the field \vec{B}_m . The second term corresponds to the jumps that

increase the magnetization by flipping the system spin down (along the axis defined by \vec{B}_m), and the third term describes the jumps that flip the system spin up, decreasing the magnetization. Since a spin flip in the system is always accompanied by a change of magnetization by one, the total magnetization

$$M = m + \frac{1}{2} (|\uparrow_m\rangle\langle\uparrow_m| - |\downarrow_m\rangle\langle\downarrow_m|), \quad (3)$$

is a conserved quantity. This implies that each time the system is prepared in an initial state, the

magnetization of the environment can change at most by one. When using a single qubit for active reservoir engineering, an iterative protocol is thus crucial to obtain a substantial manipulation of the environment, as depicted in Fig. 1. Similar to Ref. [38], the conserved quantity M can be leveraged to solve the MARE analytically. Akin to a Lindblad master equation in the secular approximation, the diagonal and the off-diagonal elements of $\partial_t \rho_m$ in the basis $\{|\sigma_m\rangle\}$, $\sigma = \uparrow, \downarrow$ decouple, and the populations evolve as,

$$\partial_t p(\downarrow, m) = \Gamma_m \left[\frac{p(\uparrow, m-1)}{V_{m-1}} - \frac{p(\downarrow, m)}{V_m} \right], \quad (4)$$

$$\partial_t p(\uparrow, m) = \Gamma_{m+1} \left[\frac{p(\downarrow, m+1)}{V_{m+1}} - \frac{p(\uparrow, m)}{V_m} \right], \quad (5)$$

where $p(\sigma, m) = \langle \sigma_m | \rho_m | \sigma_m \rangle$. The energy exchange between the system and the reservoir can thus be described by a classical rate equation for the joint probability, $p(\sigma, m)$.

To describe the scenarios illustrated in Fig. 1, a state of the form

$$\rho_m = P_m |\Psi_m\rangle\langle\Psi_m|, \quad (6)$$

is prepared repeatedly and then time-evolved by Eq. (2). For the uncorrelated states illustrated in Fig. 1, $|\Psi_m\rangle = |\downarrow_z\rangle$ and $|\Psi_m\rangle = |\uparrow_z\rangle$ have been used for the superconducting qubit and the quantum dot spin qubit respectively. The correlated states in Fig. 1 are given in Eqs. (23) and (42) below, where the corresponding protocols are discussed in depth. To simulate multiple cycles, the distribution P_m obtained at the end of a cycle is used as the initial distribution for the next cycle.

3.1 Thermodynamics of active reservoir engineering

In active quantum reservoir engineering, entropy is typically removed from the environment through the qubit. This process is constrained by the laws of thermodynamics. At step 1 in Fig. 1(a) the qubit is initialized, typically in a pure state. At step 2, the qubit evolves together with the bath through the MARE. During this process, the entropy of the system-environment compound cannot decrease. However, an increase in the entropy of the qubit allows for the entropy of the environment to decrease. At step 1 of the next cycle, the qubit is reset reducing its entropy.

Only at this stage can the entropy of the system-environment compound *decrease*, as in a Szilard engine [21, 48, 49].

For a quantitative analysis, we model the system-bath entropy using the *observational entropy* [38, 50, 51],

$$\mathcal{S}_{\text{obs}} = - \sum_{\sigma, m} p(\sigma, m) \ln p(\sigma, m) + \sum_m P_m \ln V_m. \quad (7)$$

The first term in Eq. (7) corresponds to the Shannon entropy of the joint probability $p(\sigma, m)$. It contains contributions of the marginal entropies, such as the bath Shannon entropy, as well as the mutual information [38]. The Shannon entropy of the bath,

$$\mathcal{S}_B = - \sum_m P_m \ln P_m \quad (8)$$

is central to engineering P_m —it quantifies the uncertainty about the magnetization, m . The Shannon entropy of the remaining marginal can be related to the von Neumann entropy of the system (see App. B.5),

$$\mathcal{S}(\rho_S) = - \text{tr } \rho_S \ln \rho_S. \quad (9)$$

The second term in Eq. (7) is the average of the Boltzmann entropy, $\mathcal{S}_m^{\text{Boltz}} = \ln V_m$ [50].

The MARE ensures the second law of thermodynamics, see App. B.4 for a derivation

$$\partial_t \mathcal{S}_{\text{obs}} \geq 0. \quad (10)$$

As the qubit entropy rises in step 2, the second law limits how much the Shannon entropy of the bath can decrease. In summary, the thermodynamic principles of quantum active reservoir engineering are the following.

- (i) Observational entropy is redistributed by system-environment interactions, consuming the qubit's purity to lower the Shannon entropy of the bath.
- (ii) Repeated resetting of the qubit reduces the observational entropy bit-by-bit.

3.2 Assumptions

The MARE relies on a number of assumptions that we summarize here, see Apps. A and B for more details.

First, we treat the part of the interaction that changes the magnetization perturbatively, i.e., the terms in Eq. (1) proportional to J_y and J_x . In contrast to previous approaches [38, 39], we treat the part of the interaction proportional to J_z non-perturbatively. This is particularly relevant to capture the dynamics over many cycles, when the magnetization gets substantially modified.

Second, we require the environmental decoherence time to be short compared to the energy exchange between system and bath (i.e. compared to the rates, Γ_m). In our model, environmental decoherence arises due to the spread in the frequencies ω_k but any other decoherence mechanism would have the same effect. This assumption justifies a classical description of the environment. Hence, the MARE cannot capture any effect that requires quantum coherence in the environment, such as nuclear dark states [47, 52] or the use of the environment as a quantum register [47, 53]. While the latter are experiments in which bath coherence is relevant, decoherence in the reservoir is still the reality of many state-of-the-art experiments, and our approach provides a robust benchmark of its relevance.

Third, the MARE relies on a secular approximation which assumes that the splitting between the levels of $\vec{B}_m \cdot \vec{S}$ is much larger than the rates Γ_m for all values of m .

4 Superconducting qubit

4.1 System and model

There is mounting evidence that superconducting qubits are surrounded by many two-level defects (TLSs) with different frequencies [20, 21, 54–57]. This can be captured by the Hamiltonian,

$$H = \omega_S S_z + \sum_{k=1}^N \omega_k S_z^k + V, \quad (11)$$

where the qubit (system) has frequency ω_S , the sum runs over the ensemble of TLSs and $S_z^{(k)}$ are spin-1/2 operators.

There are several conjectures about the origin of the TLS bath in the superconducting circuit [20, 21]. Here, we consider that the bath is coupled to the qubit through a Fermi-contact

hyperfine interaction [54, 56],

$$V = A \sum_{k=1}^N S_z S_z^k + A \sum_{k=1}^N (S_x S_x^k + S_y S_y^k). \quad (12)$$

We focus on cases in which V represents *weak* coupling, with hyperfine constant A . We also focus on quasi-resonant TLS, such that all frequencies ω_k are close to ω_S . Since off-resonant TLSs cannot exchange energy with the superconducting qubit, but only contribute to its dephasing, our results are also relevant in the presence of off-resonant TLSs, see App. C.1 for details. Furthermore, we disregard the spin-flip processes on the TLSs which would compete to rethermalize the TLSs bath [21, 22].

Based on the microscopic model, we find the MARE [see App. C for a derivation],

$$\begin{aligned} \partial_t \rho_m = & -i[(\omega_S + Am)S_z, \rho_m] \\ & + \kappa V_m \left(\frac{1}{2} + \frac{m}{N} \right) \left[\sigma \frac{\rho_{m-1}}{V_{m-1}} \sigma^\dagger - \frac{1}{2} \left\{ \sigma \sigma^\dagger, \frac{\rho_m}{V_m} \right\} \right] \\ & + \kappa V_m \left(\frac{1}{2} - \frac{m}{N} \right) \left[\sigma^\dagger \frac{\rho_{m+1}}{V_{m+1}} \sigma - \frac{1}{2} \left\{ \sigma^\dagger \sigma, \frac{\rho_m}{V_m} \right\} \right], \end{aligned} \quad (13)$$

where $\sigma = |\downarrow_z\rangle\langle\uparrow_z|$, κ denotes the system-bath coupling, and the volume factors are given by (assuming even N) [58, 59],

$$V_m = \frac{N!}{(N/2 + m)!(N/2 - m)!}. \quad (14)$$

The equation above has the same form as Eq. (2), with $\vec{B}_m = (\omega_S + Am)\hat{e}_z$. Equation (13) also has the same form as the one derived in [38, 39]. We note that for distributions P_m with support that is far away from the ground state or the highest excited state ($m = \mp N/2$), the factors m/N in the rates do not play a role. However, they ensure that the distribution stays within $m \in [-N/2, N/2]$ since $\Gamma_{-N/2} = \Gamma_{N/2+1} = 0$.

Previous theoretical approaches using Solomon equations [22, 60] neglect coherence in the qubit and all system-bath correlations. Neglecting coherence is reasonable in the absence of a coherent drive. However, as we discuss below, correlations are a valuable resource in active reservoir engineering.

4.2 Cooling the TLS bath

Assuming the bath is initially in a thermal state, we aim to bring it closer to the ground state.

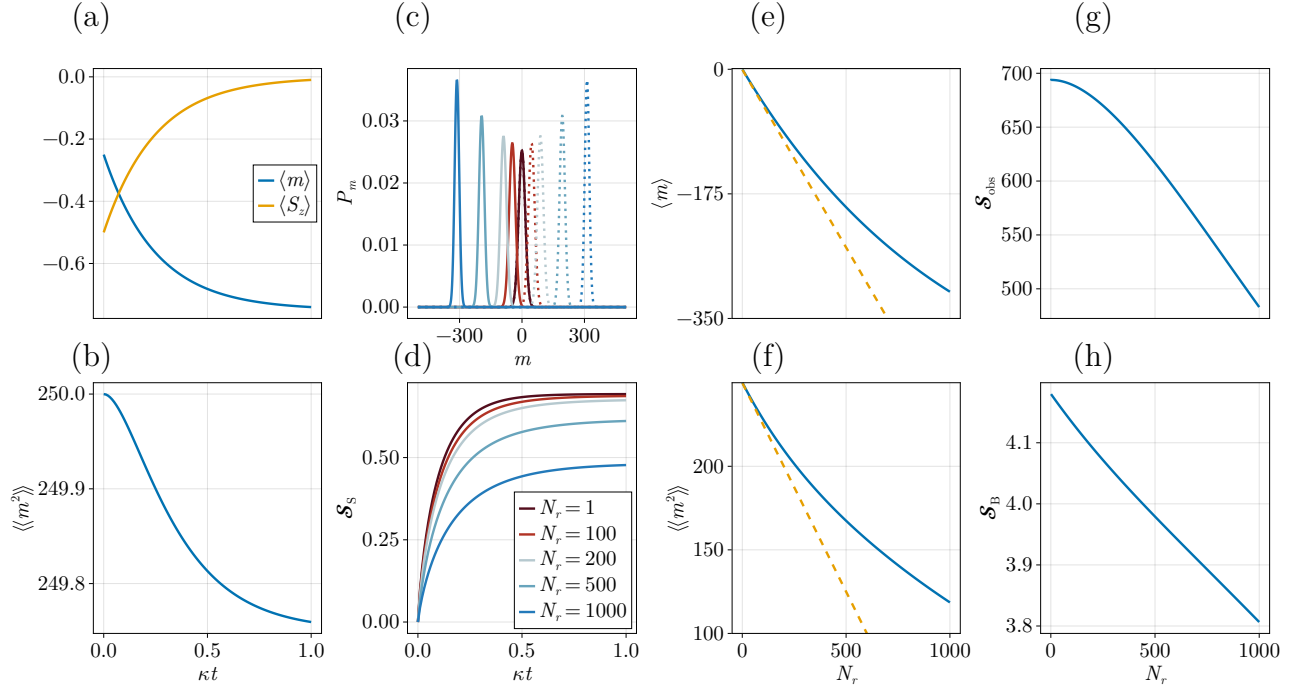


Figure 2: TLSs bath cooling. We consider a bath with $N = 1000$ TLSs and, $A/\omega_S = 0.1/N$, $\beta\omega_S = 0.001$, $\kappa/\omega_S = 10^{-5}$. (a) Change in bath (blue) and system (yellow) magnetization in the first iteration of the cooling protocol. (b) Decrease in the bath variance for the first iteration. (c) P_m at the end of N_r repetitions initializing the $|\downarrow_z\rangle$ state in the system. Dotted lines indicate population inversion protocol, in which we initialize $|\uparrow_z\rangle$ at each cycle. (d) Von Neumann entropy of the system during different iterations of the cooling protocol (c). We observe that the maximum entropy achieved decreases, witnessing the cooling of the reservoir through the qubit. (e) Average magnetization by the end of each repetition. The yellow dashed curve represents the linear term in N_r , from Eq. (21). (f) Decrease in the variance, the yellow dashed is the linear term contribution in N_r from Eq. (22). (g) As the bath cools, P_m peaks at less degenerate values of m , decreasing the observational entropy. The change in observational entropy contains relevant contributions from the change in the average Boltzmann entropy. (h) Decrease in the Shannon entropy of the bath due to narrowing of the distribution.

Since we focus on quasi-resonant TLSs, they all have an energy that is close to ω_S and the initial probability of magnetization in a thermal state is well approximated by $P_m = e^{-\beta\omega_S m} V_m / Z$. If the number of quasi-resonant spins is big enough, P_m is well approximated by a Gaussian with average μ_β and standard deviation ς_β . The aim of the cooling protocol is to move the distribution P_m towards smaller (or more negative) values of m . Ideal cooling would result in all TLSs in the ground state, which corresponds to $P_m = \delta_{m, -N/2}$. We start by investigating the equations of motion for the first and second moment of m .

From the MARE (13) we can obtain the equation of motion for the average,

$$\partial_t \langle m \rangle = -\kappa \langle m \rangle + \kappa \frac{N}{2} \langle S_z \rangle, \quad (15)$$

which is supplemented by $\partial_t \langle M \rangle = 0$, where the

conserved quantity is $M = m + S_z$. These equations can be solved. In particular, in the long-time limit we find

$$\langle m \rangle_\infty = \langle M \rangle \frac{N}{N+1}, \quad \langle S_z \rangle_\infty = \frac{\langle M \rangle}{N+1}. \quad (16)$$

The long-time behavior is determined by the conserved quantity and the number of TLSs, N .

For the second moment, we find,

$$\partial_t \langle m^2 \rangle = -2\kappa \langle m^2 \rangle + 2\kappa N \langle S_z m \rangle + \kappa \frac{N}{2}, \quad (17)$$

where we observe that it couples to the correlator with the z -magnetization of the system. We obtain for the variance in the long-time limit the following expression,

$$\begin{aligned} \langle m^2 \rangle_\infty &= \left(\langle M^2 \rangle - \frac{1}{4} \right) (1 - 1/N) - \frac{\langle M \rangle^2}{1 + 1/N^2} \\ &= \langle m^2 \rangle_0 - \langle S_z \rangle_0^2 + 2 \langle S_z m \rangle_0 + \mathcal{O}(1/N), \end{aligned} \quad (18)$$

where we used $\langle M^2 \rangle = \langle m^2 \rangle + 1/4 + 2\langle S_z m \rangle$, we introduced the notation $\langle\langle AB \rangle\rangle = \langle AB \rangle - \langle A \rangle \langle B \rangle$, and the subscript 0 denotes initial conditions. To illustrate the result, we consider the qubit to be initially in the ground state $\langle S_z \rangle_0 = -1/2$, uncorrelated with the bath which starts out in a thermal state. This results in

$$\begin{aligned}\langle m \rangle_\infty &= \mu_\beta - \frac{1}{2} + \mathcal{O}(1/N), \\ \langle S_z \rangle_\infty &= \mathcal{O}(1/N),\end{aligned}\quad (19)$$

and

$$\langle\langle m^2 \rangle\rangle_\infty = \langle\langle m^2 \rangle\rangle_\beta - \frac{1}{4} + \mathcal{O}(1/N). \quad (20)$$

From this we can conclude that, up to the finite-size contributions, we flip a single spin of the bath with probability one half; the variance decreases by $1/4$ and the average drifts by a factor of $1/2$.

We now consider the following cyclic protocol, as sketched in Fig. 1 (a). The qubit is initialized in the ground state $|\downarrow_z\rangle$, i.e. $\langle S_z \rangle_0 = -1/2$. Then, the system and bath interact for long enough that the steady-state is approached, i.e. $t \gg 1/\kappa$. Finally, the qubit is reset, destroying any system-bath correlations. This protocol is repeated N_r times, as depicted in Fig. 1 (a). According to Eq. (16) and (18), each cycle decreases the average magnetization by $1/2$ and its variance by $1/4$, until the finite size corrections that go as N_r/N become important;

$$\langle m \rangle^{(N_r)} = \mu_\beta - \frac{N_r}{2} + \mathcal{O}(N_r/N), \quad (21)$$

$$\langle\langle m^2 \rangle\rangle^{(N_r)} = \varsigma_\beta^2 - \frac{N_r}{4} + \mathcal{O}(N_r/N). \quad (22)$$

A sizeable change in the bath thus requires a number of cycles comparable to the bath size. This is illustrated in Fig. 2 (e, f). A similar protocol initializing the state $|\uparrow_z\rangle$ results in population inversion instead of cooling. Both these scenarios have been recently observed experimentally [21].

Figure 2 (d) shows the von Neumann entropy, Eq. (9) and Figs. 2 (g, h) show the Shannon, Eq. (8) and observational, Eq. (7), entropies by the end of each cycle in a cooling protocol. As expected, the Shannon entropy of the bath decreases. The observational entropy also decreases, but its decrease is steeper relative to the Shannon entropy; since P_m drifts towards a less degenerate magnetization, the contribution from the average Boltzmann entropy, $\sum_m P_m \ln V_m$,

also decreases significantly. The qubit thermalizes with the bath at each cycle and can be regarded as a thermometer; for the first cycles, its entropy reaches $\approx \log 2$ —the maximum for a qubit—, and as the bath cools the qubit reaches smaller entropies, thermalizing to a state with lower temperature.

4.3 Using correlations for engineering P_m

In this section, we investigate how a correlated state allows to narrow the bath distribution. We first consider an ideal correlated state, before turning to a class of states inspired by recent experiments on spin qubits. In this section, we do not consider the problem of creating the correlations. An example of how such correlations can be created in a different system is discussed below in Sec. 5.3. For clarity, we assume that the bath starts in a Gaussian state with $\langle m \rangle = 0$ and variance $\langle\langle m^2 \rangle\rangle = \varsigma^2$.

The jump terms in the MARE (13) indicate the ideal correlated state to achieve narrowing of P_m around $m = 0$: for $m < 0$ the system state is aligned with \vec{B}_m and for $m > 0$ it is anti-aligned. Formally, this is described by the state (for $m \neq 0$), $\rho_m^\Theta = P_m |\Psi_m^\Theta\rangle \langle \Psi_m^\Theta|$, with,

$$|\Psi_m^\Theta\rangle = \Theta_m |\downarrow_z\rangle + (1 - \Theta_m) |\uparrow_z\rangle, \quad (23)$$

where Θ_m is the Heaviside step function which is $+1$ (0) for $m > 0$ ($m < 0$). For $m = 0$, we set $\rho_0^\Theta = P_0 (|\uparrow_z\rangle \langle \uparrow_z| + |\downarrow_z\rangle \langle \downarrow_z|)/2$. With this initial state we find $\langle m S_z \rangle_0 = \langle -|m| \rangle_0$. For the considered P_m this reduces to

$$\langle\langle S_z m \rangle\rangle_0 = -\frac{\varsigma}{\sqrt{2\pi}}. \quad (24)$$

Equations (16, 18) then yield,

$$\langle m \rangle_\infty = 0, \quad (25)$$

$$\langle\langle m^2 \rangle\rangle_\infty = \varsigma^2 - \frac{\varsigma}{\sqrt{2\pi}} + \mathcal{O}(1/N). \quad (26)$$

Therefore, the anti-correlated state narrows the distribution proportionally to its standard deviation without polarizing the bath. For example, if $N = 10^4$ and $\varsigma = 50$, then a single cycle of interaction with the correlated state is comparable to the variance reduction of flipping ≈ 80 TLSs in the absence of correlations. As illustrated in Fig. 3, correlations allow for drastically narrowing the bath distribution by repeatedly initializing the state in Eq. (23). Both the entropy of the

bath as well as the variance of P_m are drastically reduced already within the first 10 cycles, i.e. for $N_r \ll N$. We note that even with the ideal state given in Eq. (23), it is not possible to perfectly narrow to $P_m = \delta_{m,0}$. The reason is that if the bath already is in the state $m = 0$, there are still processes that take the bath to $m = \pm 1$. Despite their potential for narrowing, correlations cannot enhance the drift in the magnetization of the bath (i.e., move its mean) as it still holds that at most one TLS can be flipped in each cycle.

We now consider a different class of correlated states, the Ramsey-correlated state $\rho_m^R = P_m |\Psi_m^R\rangle \langle \Psi_m^R|$, where

$$|\Psi_m^R\rangle = \cos \frac{\theta_m}{2} |\uparrow_z\rangle + \sin \frac{\theta_m}{2} |\downarrow_z\rangle, \quad (27)$$

and we highlight that the above state is the same class of states used to produce the satellite peaks in Fig. 1 (c). We assume a linear phase $\theta_m = \alpha m + \varphi$, which can be optimized to prepare an anti-correlated state.

For a Gaussian distribution $P_m = \mathcal{N}(\mu, \varsigma)$, the covariance can be computed analytically. For $\mu = 0$, we find a maximal covariance of

$$\langle\langle S_z m \rangle\rangle_0 = -\frac{\varsigma e^{-\varsigma/2}}{\sqrt{2\pi}}, \quad (28)$$

for $\alpha = 1/\varsigma$ and $\varphi = -\pi/4$. The state in Eq. (27) can be used to narrow the bath distribution, but it performs worse than the ideal case as we obtain,

$$\langle m \rangle_\infty = 0, \quad (29)$$

$$\langle\langle m^2 \rangle\rangle_\infty = \varsigma^2 - \frac{\varsigma e^{-\varsigma/2}}{\sqrt{2\pi}} + \mathcal{O}(1/N). \quad (30)$$

Beyond narrowing, the Ramsey correlated state allows the formation of satellite peaks: As a function of m , the Bloch vector of the state rotates in the xz -plane, creating points where the probability distributions P_m accumulate. Here, since $\vec{B}_m = \hat{e}_z$, the angle between \vec{B}_m and the Bloch vector of the initial state is simply θ_m . This is illustrated in Fig. 3. We note that a more slowly rotating field θ_m (i.e., smaller α) results in a narrowing of the distribution as the satellite peaks are largely offset.

Below, we discuss how states of the form of Eq. (27) can be prepared in semiconducting quantum dots using Ramsey interferometry,

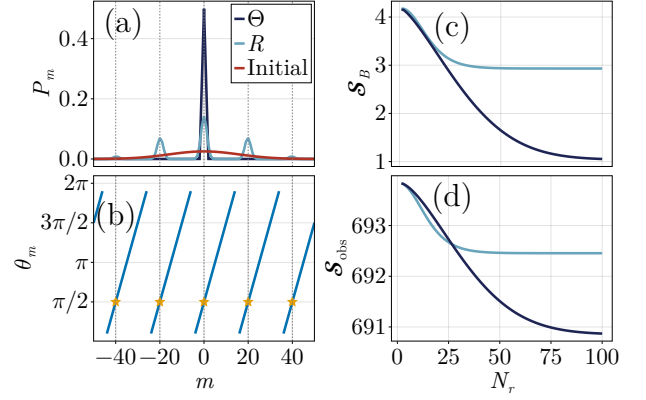


Figure 3: TLSs reservoir engineering using correlated states. We consider $N = 1000$, $A/\omega_S = 0.1/N$, $\beta = 0$, $\kappa/\omega_S = 10^{-5}$, and $\alpha = 2\pi/20$, $\varphi = \pi/2$ for the Ramsey state. (a) P_m at after $N_r = 100$ repetitions using each correlated state. We observe optimal narrowing for ρ^Θ and formation of satellite peaks in integer multiples of 20 for ρ^R . (b) Angle between the initial Ramsey state's field and \vec{B}_m . The stars denote the points at which $\theta_m = \pi/2$, where peaks in P_m are expected. (c) Shannon entropy of the bath by the end of each repetition. For the ρ^Θ we observe a huge decrease, and for ρ^R the presence of peaks limits the decrease of entropy. (d) The change of observational entropy is dominated by the Shannon entropy since the distribution is always centered at $m = 0$.

building on Ref. [27]. In superconducting qubits this preparation is challenging due to the ubiquitous dissipative processes, and may require more elaborate protocols and decoupling techniques [61].

5 Quantum-dot spin qubit

We use the MARE to understand the working principles behind a series of recent experiments in which a spin qubit is used to manipulate its nuclear environment [27, 28, 31]. These systems exhibit a wealth of interesting features at different time scales, due to the prominent role of strong system-bath interactions and system-bath correlations. Despite the complexity of these systems, we construct results based on the analytic solution of Eq. (2). Beyond reproducing the qualitative aspects of these experiments, the MARE provides a landscape of possibilities in engineering out-of-equilibrium nuclear states.

5.1 System and model

In a semiconducting quantum dot, the Zeeman-split ground state of an electron or hole can be used to implement a spin qubit. The Zeeman field also affects the nuclear spins of the semiconductor substrate which lie in the range of the spin qubit's wave-function [62] and couple to the spin qubit via hyperfine interactions. The nuclei have sharp frequencies, associated to the chemical elements in the host semiconductor [63]. For instance, in GaAs quantum dots there are two species, each with $s = 3/2$ [28], in InGaAs [31] three species with spins-3/2 and 9/2, both platforms with $N \approx 10^4 - 10^5$ nuclei, and in Si the dominant isotope has spin-1/2 [52] with $N \approx 10^3 - 10^4$ nuclei.

The interaction between the qubit and the nuclei can have many different terms [19, 64], but Eq. (1) is general enough to capture many of them. We also consider a time-dependent drive,

$$\vec{B}_0(t) = \omega_S \hat{e}_z + \Omega \cos(\omega_d t) \hat{e}_x. \quad (31)$$

We are particularly interested in the case in which the Zeeman field induces a large splitting in the system [32], i.e. $\omega_S \gg \omega_k, \Omega$. In this limit, many terms in Eq. (1) vanish under the rotating wave approximation and we obtain [27, 47, 65, 66]

$$H = \vec{B}_0 \cdot \vec{S} + \sum_{k=1}^N \omega_k I_z^k \quad (32)$$

$$+ S_z [A_c J_z + A_{nc} (J_x + J_y)],$$

$$\vec{B}_0 = \Delta \hat{e}_z + \Omega \hat{e}_x. \quad (33)$$

where we wrote the Hamiltonian in the rotating frame relative to the drive frequency. We assume the frequencies ω_k to be distributed around ω_B with a Lorentzian with width γ . We note that other decoherence mechanisms, such as spin diffusion, may alternatively be invoked to justify the MARE [27, 32, 46, 67–69].

The noncolinear terms, which are responsible for changing the magnetization of the nuclear spin bath are small in comparison to the colinear term [65, 66]. Indeed, the typical values of A_c do not allow for treating the colinear term perturbatively [32, 37, 70]. This leads to an autonomous feedback mechanism between the system and bath in which the system polarizes the bath (Knight field) and the bath polarizes the system (Overhauser field) [19, 23, 24].

From the Hamiltonian in Eq. (32), we obtain the MARE in Eq. (2) with parameters

$$\vec{B}_m = \Omega \hat{e}_x + (\Delta + A_c m) \hat{e}_z, \quad (34)$$

$$\Gamma_m = \kappa_{m,m-1} V_m r_m |\langle \downarrow_m | S_z | \uparrow_{m-1} \rangle|^2, \quad (35)$$

$$\kappa_{m,m-1} = 8\pi A_{nc}^2 \frac{\gamma}{(\omega_B - \xi_m - \xi_{m-1})^2 + \gamma^2}, \quad (36)$$

$$r_m = \frac{2}{3} s(s+1) + \frac{m}{N}, \quad (37)$$

where $\xi_m = \sqrt{\Omega^2 + (\Delta + mA_c)^2}/2$. The volume factors V_m depend on the type of nuclear spins. For spin-1/2, they are given in Eq. (14). For a bath of spin- s , we can exploit the large number of nuclei spins and use the central limit theorem to show that (see App. B.1)

$$V_m \approx \frac{[4/3Ns(s+1)]!}{[2/3Ns(s+1) + m]![2/3Ns(s+1) - m]!}, \quad (38)$$

with $m \in [-sN, sN]$. We note that in strained quantum dots, quadrupole terms in the interaction can lead to bath transitions $m \rightarrow m \pm 2$ in the MARE [19, 26, 64], and the general form of Eq. (2) has to be adapted.

There are two important features that distinguish the MARE for the quantum-dot spin qubit from the superconducting qubit scenario discussed above. First, the field \vec{B}_m rotates as a function of m . The states $|\uparrow_m\rangle$ thus obtain an explicit m -dependence with important consequences for active reservoir engineering. Second, the rates Γ_m have a strong dependence on Ω , and due to the large values of A_c , they also strongly depend on m . The rates can therefore be switched off, i.e. $\Gamma_m \rightarrow 0$ for $\Omega \rightarrow 0$. This is a consequence of the large mismatch in frequency $\omega_S \gg \omega_B$. In the absence of a drive, this mismatch prevents energy exchanges between the system and the bath. As we discuss below, this possibility of switching off energy exchanges allows to create system-bath correlations which can then be used for active reservoir engineering. We also note that the m -dependence of Γ_m implies that the environment can only exchange energy with the system when they are approximately resonant, i.e., $|\vec{B}_m| = 2\xi_m \simeq \omega_B$. Once $||\vec{B}_m| - \omega_B| \gg \gamma$, energy exchanges are no longer possible.

Note that previous theoretical works often rely on mean field type approaches, leading to *classical* rate or Fokker-Plank master equations for the

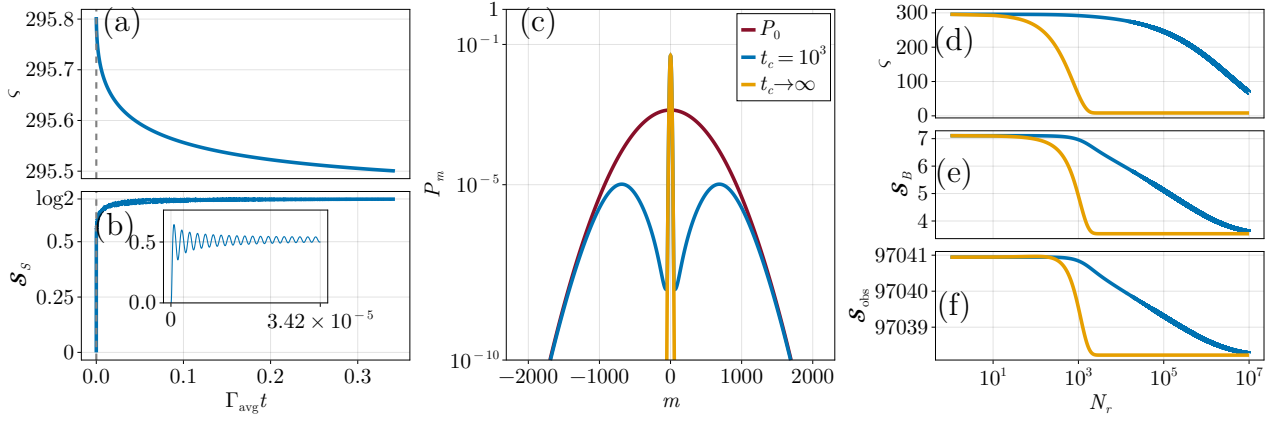


Figure 4: Narrowing of nuclear-bath with uncorrelated states. We use nominal values for the electron spin of a GaAs quantum-dot from [28], listed in Table 1. In (a–d) we simulate a single cycle of driving Rabi oscillations at Hartmann-Hahn resonance initializing state $|\uparrow_z\rangle$ in the qubit. (a) Slight decrease of the standard deviation during a single interaction cycle. (b) The von Neumann entropy of the system tends to the maximum value, but exhibits oscillations at short time scales (see inset) due to the development of sizeable system-bath correlations. In (c–f) we simulate the repeated process of narrowing the bath up to $N_r = 10^7$ repetitions. We consider resetting the spin after the system-bath compound reach the steady state, $\Gamma_{\text{avg}} t_c \gg 1$ and at finite time, $\Gamma_{\text{avg}} t_c = 3.42 \times 10^{-5}$ [vertical-dash in (a/b)], corresponding to $t_c = 1000$ ns. (c) P_m after narrowing. (d) Standard deviation at the end of each cycle. (e) Sizeable decrease in the Shannon entropy of P_m . (f) The change in observational entropy is dominated by the change in Shannon entropy.

ω_S	$2\pi \times 4.2$ GHz
ω_B	$2\pi \times 18.96$ MHz
A_c	$-2\pi \times 0.13$ MHz
A_{nc}	$2\pi \times 3 \times 10^{-3}$ MHz
γ	$\omega_B/5$
N	6.9×10^4
s	$3/2$

Table 1: We use the available reference values of GaAs quantum dot from [28, 73]. A_{nc} is estimated from the g -factor anisotropy as suggested in [47, 66], from experimental data [73]

magnetization distribution [19, 70–72]. These approaches cannot account for system-bath correlations, which are non-negligible due to the strong colinear term and useful for active reservoir engineering with initial correlations. Furthermore, Eq. (34) does not have the same form as the master equations from Refs. [38, 39], due the non-perturbative effect of A_c .

Below, we concentrate on actively engineering a spin-bath of $N = 6.9 \times 10^4$ spin- $3/2$ ^{75}As nuclei, with an initial high-temperature distribution such that $P_m \propto V_m$, using the parameters from Table 1.

5.2 Nuclear-bath narrowing without correlations

We first consider narrowing the bath distribution by repeatedly initializing the state $|\uparrow_z\rangle$ and driving Rabi oscillations at Hartmann-Hahn resonance, i.e. $\Omega = \omega_B$, as described in Sec. 2 and depicted in Fig. 1. This state results in narrowing because its Bloch vector points in the same (opposite) direction as \vec{B}_m for large negative (positive) values of m . The nonlinearities in m contained in the MARE endow the system with rich and challenging physics. Yet, due to the conserved quantity, the MARE can be analytically solved by the method from Ref. [38], as we explain in App. B.3.

After each initialization of the system, the variance of P_m and the bath entropy decrease, while the system entropy increases, see Fig. 4 (b–d). The relevant time-scale for the system-bath interaction is estimated as,

$$\Gamma_{\text{avg}} = \frac{1}{2sN} \sum_{m=-sN}^{sN} \Gamma_m. \quad (39)$$

While the quantities of the bath exhibit a monotonic evolution to their steady-state values, the von Neumann entropy of the system shows an intricate behavior, as seen in Fig. 4 (b). In

general, the system density matrix evolves in a non-Markovian fashion [35, 36, 38]. Compared to the superconducting scenario above, the non-Markovianity is enhanced because the direction of the magnetic field \vec{B}_m depends on the previous energy exchanges between system and bath.

By repeatedly initializing the system in the state $|\uparrow_z\rangle$, significant narrowing can be achieved as illustrated in Fig. 4(d-f). We consider $N_r = 10^7$ initializations, where the system exchanges energy with the environment for the duration of $\Gamma_{\text{avg}} t_c = 3.42 \times 10^{-5}$ (corresponding to $t_c = 1000$ ns). We find that it takes $N_r \approx N$ cycles for a significant reduction of the variance $\langle m^2 \rangle$ and the bath entropy. Although the initial and final distributions are approximately Gaussian, the intermediate steps can contain non-Gaussian features. In Fig. 4(e) we observe a sensible decrease in the bath Shannon entropy. The observational entropy in Fig. 4(f) is dominated by the large average Boltzmann entropy, but its change is dominated by the change in Shannon entropy, which can be seen by comparing with (f).

Notably, although using $t_c \rightarrow \infty$ is apparently more efficient in terms of the number of cycles needed to engineer the reservoir, in practice this might be much less convenient. Indeed, we estimate that the time to reach the steady state is of the order seconds and iterating many repetitions over such long times can be forbidding. That is, in practice, a compromise between number of repetitions and driving time has to be found.

5.3 Active engineering with correlations

With the goal of narrowing the bath distribution in mind, we now discuss how to use correlated states. As for the superconducting qubit case, we first note that the idealized state for narrowing is given by

$$|\Psi_m^\Theta\rangle = \Theta_m |\downarrow_m\rangle + (1 - \Theta_m) |\uparrow_m\rangle. \quad (40)$$

This state has a Bloch vector that is (anti-)parallel with the field \vec{B}_m for negative (positive) values of m . Therefore, it results in an increase in magnetization for $m < 0$ and in a decrease of magnetization for $m > 0$. However, we are not aware of a strategy to prepare this state in an experiment.

Therefore, we turn to the quantum sensing protocol introduced in Ref. [27], which relies on Ramsey interferometry [74] to prepare correlated

states. According to Eq. (34), the dissipative terms are negligible whenever we operate the qubit far from Hartmann-Hahn resonance; however, the Overhauser field is always present, and allows the qubit to sense the bath magnetization. For $\Omega = 0$, the MARE reduces to

$$\partial_t \rho_m = -i[\vec{B}_m \cdot \vec{S}, \rho_m]. \quad (41)$$

Preparing the state $|\psi_m\rangle = (|\uparrow_z\rangle + i|\downarrow_z\rangle)/\sqrt{2}$, letting it evolve according to Eq. (41), and rotating the state back to the xz -plane (the plane in which \vec{B}_m lies), we obtain the state

$$|\Psi_m^R\rangle = \cos(A_c m \tau) |\uparrow_z\rangle + \sin(|A_c| m \tau) |\downarrow_z\rangle, \quad (42)$$

where we set $\Delta = 0$ and τ denotes the evolution time. Due to the distribution of the magnetization, this evolution results in decoherence of the spin qubit $\rho_S = \sum_m P_m |\Psi_m^R\rangle \langle \Psi_m^R|$. By plotting the probability of finding the qubit in the $|\uparrow_z\rangle$ state, the coherence time of the qubit can be determined. This is illustrated in Fig. 6(c), and discussed below. For a Gaussian distribution $P_m \approx \mathcal{N}(\mu = 0, \varsigma)$, the coherence time is given by $T_2^* = \sqrt{2}/(\varsigma |A_c| \tau)$.

Here, we consider a repeated initialization of the state in Eq. (42) with $\tau = (100|A_c|)^{-1}$. Since the Bloch vector of this state, as well as \vec{B}_m , rotate as a function of m , we find multiple regions where the Bloch vector is (anti-)parallel to the field. This results in multiple peaks in P_m when the state is initialized many times, see Fig. 5. These peaks occur when the Bloch vector of the state is perpendicular to the field \vec{B}_m .

Finally, we illustrate how the state in Eq. (42) can be exploited for narrowing P_m , as done experimentally in Refs. [27, 28, 31]. To this end, we note that the location of the satellite peaks (at $m \neq 0$) depends on the time τ . By sweeping τ , i.e., using a different τ_j for each initialization, these satellite peaks can be suppressed, as in Fig. 6. We consider a protocol where τ_j is increased from $\tau_i = 0.025|A_c|^{-1}$ to $\tau_f = 0.1|A_c|^{-1}$ in 100 steps. These 100 preparations are then repeated 10^7 times.

As seen in Fig. 6, this protocol (R , light-blue curves) results in narrowing and a coherence time that is comparable to what is obtained from the ideal state in Eq. (40) (dark blue curves). We also compare the results with those obtained from repeated initialization of uncorrelated states, $|\uparrow_z\rangle$,

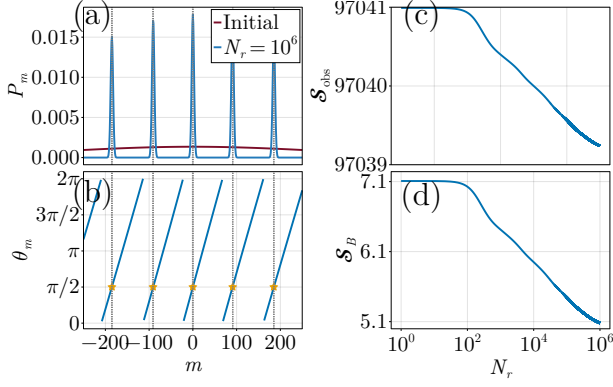


Figure 5: Active reservoir engineering with Ramsey-correlated states. Fixed parameters from Table 1 and sensing time, $|A_c|\tau = 1/100$. (a) Spiked distribution after 10^6 repetitions and initial distribution. (b) θ_m is the angle between \vec{B}_m and the Bloch vector of $|\Psi_m^R\rangle$. The peaks in (a) are formed every time the angle is $\pi/2$. (c) Decrease in observational entropy. (d) The decrease in observational entropy is dominated by the decrease in Shannon entropy of the bath. Although many peaks remain, the uncertainty on the value of m reduces.

see also Fig. 4. The coherence time is determined through the Ramsey visibility [74],

$$\mathcal{V}_R = \frac{1}{2} - \frac{1}{2}\langle \cos(\tau A_c m) \rangle. \quad (43)$$

Where we considered the average with respect to each of the probabilities obtained from different protocols. Figure 6 (c) shows that the ideal state, Θ , results in a value of $T_2^* = 2021$ ns that is only around 30% longer than the Ramsey protocol, which gives $T_2^* = 1638$ ns. This is quite remarkable considering that there is no known protocol to prepare Eq. (40) whereas the protocol relying on Ramsey interferometry with varying τ_j has been implemented experimentally [27, 28, 31]. However, the ideal state typically allows for reaching the stationary limit of $N_r \rightarrow \infty$ faster, as illustrated in Fig. 6 (b). Notably, the correlated states outperform the preparation of $|\uparrow_z\rangle$ by an order of magnitude in the coherence time.

Despite using a simplified model (e.g. a single nuclear species) the MARE predicts similar coherence times to the ones observed experimentally using analogous narrowing protocols in Ref. [28].

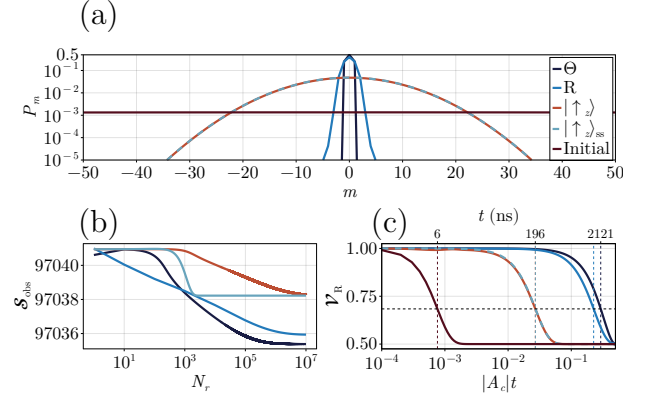


Figure 6: Engineering narrow nuclear states. We compare distinct strategies using correlated and uncorrelated states to create a concentration of probability at $m = 0$. The dark-blue (Θ) represents the ideal protocol, with initial state in Eq. (40). The light blue indicates the Ramsey protocol (R), in which the sensing time is varied between the cycles; for this protocol $t_c = 10^4$, $\tau \in [0.02/|A_c|, 0.1/|A_c|]$ with $N_r = 100$ steps in each run. The overlapping light blue and light red curves correspond to repeated initialization of $|\uparrow_z\rangle$ for a finite t_c and for $t_c \rightarrow \infty$ (subscript ss), see also Fig. 4. Dark red indicates the initial bath distribution. (a) P_m obtained after $N_r = 10^7$ repetitions of each protocol. (b) Observational entropy as a function of N_r . (c) Ramsey visibility, \mathcal{V}_R , characterizing the coherence time, T_2^* , of the spin qubit after narrowing.

6 Conclusions and outlook

We have developed a theoretical framework for active reservoir engineering. Our framework provides an intuitive understanding for how repeated preparation of a controlled quantum system can be used to manipulate its environment and drive it towards a target state. It recovers the qualitative behavior observed experimentally in different platforms, including superconducting qubits coupled to an environment of TLSs [21], as well as spin qubits in quantum dots coupled to nuclear spins [27, 28, 31]. Our framework shows that the dynamics of the system and the reservoir is determined by the effective field felt by the system and the Bloch vector of the prepared state. Knowing the effective field as a function of the environment magnetization thus allows for developing effective strategies for active reservoir engineering.

Our framework enables the development of novel strategies for active reservoir engineering. Furthermore, it may provide insight into the Hamiltonian underlying an experiment. A

promising avenue in this direction is to use the periodic narrowing of the nuclear spin distribution to map out the direction of the effective field as a function of magnetization and the underlying bath spectral density. To make quantitative predictions, the approximations underlying our framework have to be carefully examined for the experiment of interest. In particular, long coherence times in the environment may prevent a classical description of the magnetization. In this case, the MARE provides a relevant benchmark to determine if the observed behavior of the reservoir is truly nonclassical and cannot be captured by our approach. In addition, the repeated initialization of the system may require to investigate time-scales shorter than the coherence time of the reservoir. This could be achieved by combining our framework with the coarse-graining approach for Markovian master equations [75]. In future work, we will also show how the MARE can be expanded to derive a quantum Fokker-Planck master equation, akin to Ref. [76], for a large bath with short-range jumps. Another promising avenue is provided by modifying the projector operators, allowing for coherent features in the reservoir [36] to describe dark states [47, 52], and include further non-perturbative contributions [43, 54, 77]. The MARE describes a quantum system interacting with a reservoir that decoheres with respect to a given basis; it could be applied to contexts other than active reservoir engineering, such as the emergence of classical outcomes in a detector—treated as a reservoir—coupled to a quantum system [78].

Acknowledgements

We acknowledge fruitful discussions with G. N. Nguyen, M. R. Hogg, R. J. Warburton, L. I. Glazman, G. Haack, N. Brunner, N. Gisin, D. Basko, A. Riera-Campenya, and P. Strasberg. This work was supported by the Swiss National Science Foundation (Eccellenza Professorial Fellowship PCEFP2.194268). M.B. acknowledges funding from the European Research Council (ERC) under the European Union’s Horizon 2020 research and innovation program (Grant agreement No. 101002955 – CONQUER).

References

- [1] J. F. Poyatos, J. I. Cirac, and P. Zoller, *Phys. Rev. Lett.* **77**, 4728 (1996).
- [2] F. Verstraete, M. M. Wolf, and J. I. Cirac, *Nat. Phys.* **5**, 633 (2009).
- [3] P. M. Harrington, E. J. Mueller, and K. W. Murch, *Nat. Rev. Phys.* **4**, 660 (2022).
- [4] A. Metelmann and A. A. Clerk, *Phys. Rev. X* **5**, 021025 (2015).
- [5] C.-E. Bardyn, M. A. Baranov, C. V. Kraus, E. Rico, A. İmamoğlu, P. Zoller, and S. Diehl, *New J. Phys.* **15**, 085001 (2013).
- [6] Z. Leghtas, S. Touzard, I. M. Pop, A. Kou, B. Vlastakis, A. Petrenko, K. M. Sliwa, A. Narla, S. Shankar, M. J. Hatridge, M. Reagor, L. Frunzio, R. J. Schoelkopf, M. Mirrahimi, and M. H. Devoret, *Science* **347**, 853 (2015).
- [7] R. Lescanne, M. Villiers, T. Peronnin, A. Sarlette, M. Delbecq, B. Huard, T. Kontos, M. Mirrahimi, and Z. Leghtas, *Nat. Phys.* **16**, 509 (2020).
- [8] J. M. Gertler, B. Baker, J. Li, S. Shirol, J. Koch, and C. Wang, *Nature* **590**, 243 (2021).
- [9] Q. Xu, G. Zheng, Y.-X. Wang, P. Zoller, A. A. Clerk, and L. Jiang, *npj Quantum Inf.* **9**, 78 (2023).
- [10] B. Kraus, H. P. Büchler, S. Diehl, A. Kantian, A. Micheli, and P. Zoller, *Phys. Rev. A* **78**, 042307 (2008).
- [11] S. Diehl, A. Micheli, A. Kantian, B. Kraus, H. P. Büchler, and P. Zoller, *Nature Physics* **4**, 878 (2008).
- [12] J. T. Barreiro, M. Müller, P. Schindler, D. Nigg, T. Monz, M. Chwalla, M. Hennrich, C. F. Roos, P. Zoller, and R. Blatt, *Nature* **470**, 486 (2011).
- [13] Y. Lin, J. P. Gaebler, F. Reiter, T. R. Tan, R. Bowler, A. S. Sørensen, D. Leibfried, and D. J. Wineland, *Nature* **504**, 415 (2013).
- [14] Z. Leghtas, U. Vool, S. Shankar, M. Hatridge, S. M. Girvin, M. H. Devoret, and M. Mirrahimi, *Phys. Rev. A* **88**, 023849 (2013).
- [15] P. Zapletal, A. Nunnenkamp, and M. Brunelli, *PRX Quantum* **3**, 010301 (2022).
- [16] A. Kronwald, F. Marquardt, and A. A. Clerk, *Phys. Rev. A* **88**, 063833 (2013).

- [17] E. E. Wollman, C. U. Lei, A. J. Weinstein, J. Suh, A. Kronwald, F. Marquardt, A. A. Clerk, and K. C. Schwab, *Science* **349**, 952 (2015).
- [18] R. Dassonneville, R. Assouly, T. Peronnin, A. Clerk, A. Bienfait, and B. Huard, *PRX Quantum* **2**, 020323 (2021).
- [19] B. Urbaszek, X. Marie, T. Amand, O. Krebs, P. Voisin, P. Maletinsky, A. Högele, and A. Imamoglu, *Rev. Mod. Phys.* **85**, 79 (2013).
- [20] P. V. Klimov, J. Kelly, Z. Chen, M. Neeley, A. Megrant, B. Burkett, R. Barends, K. Arya, B. Chiaro, Y. Chen, A. Dunsworth, A. Fowler, B. Foxen, C. Gidney, M. Giustina, R. Graff, T. Huang, E. Jeffrey, E. Lucero, J. Y. Mutus, O. Naaman, C. Neill, C. Quintana, P. Roushan, D. Sank, A. Vainsencher, J. Wenner, T. C. White, S. Boixo, R. Babbush, V. N. Smelyanskiy, H. Neven, and J. M. Martinis, *Phys. Rev. Lett.* **121**, 090502 (2018).
- [21] M. Spiecker, P. Paluch, N. Gosling, N. Drucker, S. Matityahu, D. Gusenkova, S. Günzler, D. Rieger, I. Takmakov, F. Valenti, P. Winkel, R. Gebauer, O. Sander, G. Catelani, A. Shnirman, A. V. Ustinov, W. Wernsdorfer, Y. Cohen, and I. M. Pop, *Nat. Phys.* **19**, 1320 (2023).
- [22] M. Spiecker, A. I. Pavlov, A. Shnirman, and I. M. Pop, *Phys. Rev. A* **109**, 052218 (2024).
- [23] D. Stepanenko, G. Burkard, G. Giedke, and A. Imamoglu, *Phys. Rev. Lett.* **96**, 136401 (2006).
- [24] C. W. Lai, P. Maletinsky, A. Badolato, and A. Imamoglu, *Phys. Rev. Lett.* **96**, 167403 (2006).
- [25] C. Latta, A. Högele, Y. Zhao, A. N. Vamivakas, P. Maletinsky, M. Kroner, J. Dreiser, I. Carusotto, A. Badolato, D. Schuh, W. Wegscheider, M. Atatüre, and A. Imamoglu, *Nat. Phys.* **5**, 758 (2009).
- [26] D. A. Gangloff, G. Éthier-Majcher, C. Lang, E. V. Denning, J. H. Bodey, D. M. Jackson, E. Clarke, M. Hugues, C. L. Gall, and M. Atatüre, *Science* **364**, 62 (2019).
- [27] D. M. Jackson, U. Haeusler, L. Zaporski, J. H. Bodey, N. Shofer, E. Clarke, M. Hugues, M. Atatüre, C. Le Gall, and D. A. Gangloff, *Phys. Rev. X* **12**, 031014 (2022).
- [28] G. N. Nguyen, C. Spinnler, M. R. Hogg, L. Zhai, A. Javadi, C. A. Schrader, M. Erbe, M. Wyss, J. Ritzmann, H.-G. Babin, A. D. Wieck, A. Ludwig, and R. J. Warburton, *Phys. Rev. Lett.* **131**, 210805 (2023).
- [29] J. P. King, P. J. Coles, and J. A. Reimer, *Phys. Rev. B* **81**, 073201 (2010).
- [30] S. Khandelwal, S. Kumar, N. Palazzo, G. Haack, and M. Chipaux, *Phys. Rev. B* **108**, 174418 (2023).
- [31] M. Hogg, N. Antoniadis, M. Marczak, G. Nguyen, T. Baltisberger, A. Javadi, R. Schott, S. Valentin, A. Wieck, A. Ludwig, and R. Warburton, Fast optical control of a coherent hole spin in a microcavity (2024), [arXiv:2407.18876 \[quant-ph\]](https://arxiv.org/abs/2407.18876).
- [32] W. A. Coish, J. Fischer, and D. Loss, *Phys. Rev. B* **77**, 125329 (2008).
- [33] M. Esposito and P. Gaspard, *Phys. Rev. E* **68**, 066112 (2003).
- [34] J. Fischer and H.-P. Breuer, *Phys. Rev. A* **76**, 052119 (2007).
- [35] H.-P. Breuer, J. Gemmer, and M. Michel, *Phys. Rev. E* **73**, 016139 (2006).
- [36] H.-P. Breuer, *Phys. Rev. A* **75**, 022103 (2007).
- [37] E. Barnes, L. Cywiński, and S. Das Sarma, *Phys. Rev. Lett.* **109**, 140403 (2012).
- [38] A. Riera-Campenya, A. Sanpera, and P. Strasberg, *PRX Quantum* **2**, 010340 (2021).
- [39] A. Riera-Campenya, A. Sanpera, and P. Strasberg, *Phys. Rev. E* **105**, 054119 (2022).
- [40] Gaudin, M., *J. Phys. France* **37**, 1087 (1976).
- [41] D. Garajew, *J. Math. Phys.* **43**, 5732 (2002).
- [42] J. Schliemann, A. Khaetskii, and D. Loss, *J. Phys. : Cond. Mat.* **15**, R1809 (2003).
- [43] O. Tsyplatyev and D. Loss, *Phys. Rev. Lett.* **106**, 106803 (2011).
- [44] W.-B. He, S. Chesi, H.-Q. Lin, and X.-W. Guan, *Communications in Theoretical Physics* **74**, 095102 (2022).
- [45] A. Ruskuc, C.-J. Wu, J. Rochman, J. Choi, and A. Faraon, *Nature* **602**, 408 (2022).
- [46] J. Hildmann, E. Kavousanaki, G. Burkard, and H. Ribeiro, *Phys. Rev. B* **89**, 205302 (2014).
- [47] M. H. Appel, A. Ghorbal, N. Shofer, L. Zaporski, S. Manna, S. F. C. da Silva, U. Haeusler, C. Le Gall, A. Rastelli, D. A.

- Gangloff, and M. Atatüre, *Nat. Phys.* **21**, 368 (2025).
- [48] L. Szilard, *Z. Phys.* **53**, 840 (1929).
- [49] H. S. Leff and A. F. Rex, eds., *Entropy, Information, Computing* (Princeton University Press, Princeton, 1990).
- [50] D. Šafránek, J. M. Deutsch, and A. Aguirre, *Phys. Rev. A* **99**, 010101 (2019).
- [51] P. Strasberg and A. Winter, *PRX Quantum* **2**, 030202 (2021).
- [52] X. Cai, H. Y. Walelign, and J. M. Nichol, *Nat. Phys.* **21**, 536 (2025).
- [53] E. V. Denning, D. A. Gangloff, M. Atatüre, J. Mørk, and C. Le Gall, *Phys. Rev. Lett.* **123**, 140502 (2019).
- [54] J. Wu and C. C. Yu, *Phys. Rev. Lett.* **108**, 247001 (2012).
- [55] Y. Shalibo, Y. Rofo, D. Shwa, F. Zeides, M. Neeley, J. M. Martinis, and N. Katz, *Phys. Rev. Lett.* **105**, 177001 (2010).
- [56] C. M. Quintana, Y. Chen, D. Sank, A. G. Petukhov, T. C. White, D. Kafri, B. Chiaro, A. Megrant, R. Barends, B. Campbell, Z. Chen, A. Dunsworth, A. G. Fowler, R. Graff, E. Jeffrey, J. Kelly, E. Lucero, J. Y. Mutus, M. Neeley, C. Neill, P. J. J. O'Malley, P. Roushan, A. Shabani, V. N. Smelyanskiy, A. Vainsencher, J. Wenner, H. Neven, and J. M. Martinis, *Phys. Rev. Lett.* **118**, 057702 (2017).
- [57] F. Yan, S. Gustavsson, A. Kamal, J. Birenbaum, A. P. Sears, D. Hover, T. J. Gudmundsen, D. Rosenberg, G. Samach, S. Weber, J. L. Yoder, T. P. Orlando, J. Clarke, A. J. Kerman, and W. D. Oliver, *Nat. Commun.* **7**, 12964 (2016).
- [58] S. R. Salinas, *Introduction to statistical physics*, Graduate texts in contemporary physics (Springer, New York, 2001).
- [59] R. H. Dicke, *Phys. Rev.* **93**, 99 (1954).
- [60] I. Solomon, *Phys. Rev.* **99**, 559 (1955).
- [61] L. Cywiński, R. M. Lutchyn, C. P. Nave, and S. Das Sarma, *Phys. Rev. B* **77**, 174509 (2008).
- [62] W. A. Coish and D. Loss, *Phys. Rev. B* **70**, 195340 (2004).
- [63] L. Cywiński, W. M. Witzel, and S. Das Sarma, *Phys. Rev. B* **79**, 245314 (2009).
- [64] W. A. Coish and J. Baugh, *Phys. Stat. Sol. (b)* **246**, 2203 (2009).
- [65] M. S. Rudner and L. S. Levitov, *Phys. Rev. Lett.* **99**, 036602 (2007).
- [66] N. Shofer, L. Zaporski, M. Hayhurst Appel, S. Manna, S. Covre da Silva, A. Ghorbal, U. Haeusler, A. Rastelli, C. Le Gall, M. Gawelczyk, M. Atatüre, and D. A. Gangloff, *Phys. Rev. X* **15**, 021004 (2025).
- [67] D. Paget, G. Lampel, B. Sapoval, and V. I. Safarov, *Phys. Rev. B* **15**, 5780 (1977).
- [68] D. Paget, *Phys. Rev. B* **25**, 4444 (1982).
- [69] G. Wüst, M. Munsch, F. Maier, A. V. Kuhlmann, A. Ludwig, A. D. Wieck, D. Loss, M. Poggio, and R. J. Warburton, *Nat. Nano.* **11**, 885 (2016).
- [70] A. Högele, M. Kroner, C. Latta, M. Claassen, I. Carusotto, C. Bulutay, and A. Imamoglu, *Phys. Rev. Lett.* **108**, 197403 (2012).
- [71] J. Danon and Y. V. Nazarov, *Phys. Rev. Lett.* **100**, 056603 (2008).
- [72] W. Yang and L. J. Sham, *Phys. Rev. B* **88**, 235304 (2013).
- [73] G. N. B. Nguyen, *Coherent photons and coherent spins in a GaAs quantum dot* (Universität Basel, 2024).
- [74] C. L. Degen, F. Reinhard, and P. Cappellaro, *Rev. Mod. Phys.* **89**, 035002 (2017).
- [75] G. Schaller and T. Brandes, *Phys. Rev. A* **78**, 022106 (2008).
- [76] B. Annby-Andersson, F. Bakhshinezhad, D. Bhattacharyya, G. De Sousa, C. Jarzynski, P. Samuelsson, and P. P. Potts, *Phys. Rev. Lett.* **129**, 050401 (2022).
- [77] E. Barnes, L. Cywiński, and S. Das Sarma, *Phys. Rev. B* **84**, 155315 (2011).
- [78] A. E. Allahverdyan, R. Balian, and T. M. Nieuwenhuizen, *Phys. Rep.* **525**, 1 (2013).
- [79] S. Nakajima, *Prog. Theor. Phys.* **20**, 948 (1958).
- [80] R. Zwanzig, *J. Chem. Phys.* **33**, 1338 (1960).
- [81] H.-P. Breuer and F. Petruccione, *The Theory of Open Quantum Systems* (Oxford University Press, 2007).
- [82] L. Mandel and E. Wolf, Collective atomic interactions, in *Optical Coherence and Quantum Optics* (Cambridge University Press, 1995) p. 805–859.
- [83] P. P. Potts, Quantum thermodynamics (2024), [arXiv:2406.19206 \[quant-ph\]](https://arxiv.org/abs/2406.19206).
- [84] T. Cover and J. Thomas, Entropy, relative entropy, and mutual information, in *Ele-*

- ments of Information Theory* (John Wiley and Sons, Ltd, 2005) Chap. 2, pp. 13–55.
- [85] A. Streltsov, G. Adesso, and M. B. Plenio, *Rev. Mod. Phys.* **89**, 041003 (2017).
- [86] G. Lindblad, *Com. Math. Phys.* **40**, 147 (1975).
- [87] G. T. Landi, Eigenoperator approach to Schrieffer-Wolff perturbation theory and dispersive interactions (2024), arXiv:2409.10656 [quant-ph] .

A General Theory

In this Section we provide a derivation of the MARE for general quantum systems. We discuss important properties and assumptions and provide a general quantum Fokker-Planck master equation via jump-length expansion.

A.1 Microscopic derivation of the generalized MARE

The MARE is a generalization of the results of Ref. [38, 39], in which we include the part of the system-bath interaction that does not lead to jumps in the bath nonperturbatively.

Projectors and rotating frame.—We consider a system and an environment (bath) with Hamiltonian,

$$H = H_S + H_B + H_{SB}. \quad (44)$$

We further consider a bath observable with spectral decomposition

$$M_B = \sum_m m \Pi_m, \quad (45)$$

that commutes with the bath Hamiltonian, $[M_B, H_B] = [\Pi_m, H_B] = 0$. This will be the bath observable that we keep track of. In the main text, this corresponds to the magnetization and in Refs. [38, 39] M_B corresponds to a coarse-grained version of H_B . Here we leave it general. The operators Π_m are orthogonal projection operators, $\Pi_m \Pi_{m'} = \delta_{m,m'} \Pi_m$, but not necessarily rank-1; their rank is denoted $V_m = \text{tr} \Pi_m$ and called *volume factor*. With the help of these quantities, we introduce the correlated projector superoperator,

$$\mathcal{P}\rho = \sum_m \rho_m \otimes \frac{\Pi_m}{V_m}, \quad \rho_m = \text{tr}_B \{\Pi_m \rho\}. \quad (46)$$

Note that when m corresponds to a coarse-grained energy, then the state Π_m/V_m denotes the microcanonical ensemble [38].

We now decompose the H_{SB} term in the Hamiltonian in two parts,

$$H_{SB} = \delta H + V, \quad \delta H = \sum_m \langle H_{SB} \rangle_m \Pi_m, \quad (47)$$

where we introduced the microcanonical average $\langle \circ \rangle_m = \text{tr}_B \{\circ \Pi_m / V_m\}$.

We will only treat V perturbatively (not to be confused with the volume factors, V_m). The rest of the interaction, δH , is treated non-perturbatively. To this end, we consider the unitary operator,

$$R(t) = e^{it(H_S + H_B + \delta H)} = e^{it(H_S + \delta H)} e^{itH_B}, \quad (48)$$

where we note that, in general $[H_S, \delta H] \neq 0$. We may write

$$R(t) = \sum_m R_m(t) \Pi_m e^{itH_B}, \quad (49)$$

with

$$R_m(t) = e^{itH_m}, \quad H_m = H_S + \langle H_{SB} \rangle_m. \quad (50)$$

If the system has only two levels, we can always write $H_m = \vec{B}_m \cdot \vec{S}$ where $S_{x,y,z}$ are spin operators—we will not make this assumption during the derivation below.

We now consider the density matrix in the rotating frame

$$\tilde{\rho}(t) = R(t)\rho(t)R^\dagger(t), \quad \partial_t \tilde{\rho}(t) = \mathcal{V}(t)\tilde{\rho}(t), \quad (51)$$

with $\mathcal{V}(t) \circ = -i[\tilde{V}(t), \circ]$, and $\tilde{V}(t) = R(t)VR^\dagger(t)$. Using $\mathcal{Q} = 1 - \mathcal{P}$, one may then formally solve the equation $\partial_t \mathcal{Q}\tilde{\rho}$ and plug the solution into the equation $\partial_t \mathcal{P}\tilde{\rho}$. Using $\mathcal{P}\mathcal{V}\mathcal{P} = 0$, this results in the standard Nakajima-Zwanzig equation [79, 80],

$$\partial_t \mathcal{P}\tilde{\rho} = \int_0^t dt' \mathcal{P}\mathcal{V}(t)\mathcal{G}(t, t')\mathcal{Q}\mathcal{V}(t')\tilde{\rho}(t'), \quad (52)$$

where $\mathcal{G}(t, t') = \mathcal{T} \exp\left\{i \int_{t'}^t ds \mathcal{Q}\mathcal{V}(s)\right\}$ is the memory kernel and \mathcal{T} denotes time ordering.

Weak coupling.— We now perturbatively expand the Nakajima-Zwanzig equation in V . The lowest non-zero order gives,

$$\partial_t \tilde{\rho}_m = - \sum_{m'} \int_0^t dt' \text{tr}_B \left\{ \Pi_m \left[\tilde{V}(t), \left[\tilde{V}(t'), \tilde{\rho}_{m'}(t') \otimes \frac{\Pi_{m'}}{V_{m'}} \right] \right] \right\}. \quad (53)$$

It is always possible to write the interaction in the form

$$V = \sum_{\alpha} S_{\alpha} \otimes B_{\alpha}, \quad (54)$$

where S_{α} acts on the system and B_{α} on the bath. We then obtain,

$$\tilde{V}(t) = \sum_{\alpha, m, m'} \tilde{S}_{mm'}^{\alpha} \otimes \Pi_m \tilde{B}_{\alpha} \Pi_{m'}, \quad (55)$$

where we introduced $\tilde{B}_{\alpha}(t) = e^{itH_B} B_{\alpha} e^{-itH_B}$, $\tilde{S}_{mm'}^{\alpha} = R_m(t) S_{\alpha} R_{m'}^{\dagger}(t)$. Note that, although $R(t)$ in general does not preserve the original product structure of the interaction, mixing operators from system and bath, the product can be restored at the cost of introducing the sum over m, m' . This is the immediate consequence of treating $\langle H_{SB} \rangle_m$ exactly, which imprints a dependence on m on the transitions in the system induced by the operators $\tilde{S}_{mm'}^{\alpha}$. Substituting Eq. (55) in Eq. (53) we obtain,

$$\partial_t \tilde{\rho}_m = \sum_{m' \alpha \beta} \int_0^t dt' C_{mm'}^{\alpha \beta}(t' - t) \left[\tilde{S}_{mm'}^{\alpha}(t) \frac{\tilde{\rho}_{m'}(t')}{V_{m'}} \tilde{S}_{m'm}^{\beta}(t') - \tilde{S}_{mm'}^{\alpha}(t) \tilde{S}_{m'm}^{\beta}(t') \frac{\tilde{\rho}_m(t')}{V_m} \right] + \text{h.c.} \quad (56)$$

where we introduced the microcanonical correlation functions,

$$C_{mm'}^{\alpha \beta}(t - t') = \text{tr}_B \left\{ \Pi_m \tilde{B}_{\alpha}(t) \Pi_{m'} \tilde{B}_{\beta}(t') \right\} = \text{tr}_B \left\{ \Pi_m \tilde{B}_{\alpha}(t - t') \Pi_{m'} B_{\beta}(0) \right\}.$$

The dependence on $t - t'$ instead of t, t' is a consequence of $[\Pi_m, H_B] = 0$. The correlation functions have the property,

$$C_{mm'}^{\alpha \beta}(t - t') = C_{m'm}^{\beta \alpha}[-(t - t')]. \quad (57)$$

The next steps follow closely the microscopic derivation of a Lindblad master equation. We will perform the Markov and secular approximations [81].

Markov approximation.— Assuming that the microcanonical correlation functions decay on a time-scale that is much shorter than the characteristic time over which $\tilde{\rho}_m$ changes, we can substitute $\tilde{\rho}_m(t')$ with $\tilde{\rho}_m(t)$ in Eq. (56). Further changing variables to $\tau = t - t'$, we find

$$\partial_t \tilde{\rho}_m \approx \sum_{m' \alpha \beta} \int_0^{\infty} d\tau C_{mm'}^{\alpha \beta}(\tau) \left[\tilde{S}_{mm'}^{\alpha}(t) \frac{\tilde{\rho}_{m'}(t)}{V_{m'}} \tilde{S}_{m'm}^{\beta}(t - \tau) - \tilde{S}_{mm'}^{\alpha}(t) \tilde{S}_{m'm}^{\beta}(t - \tau) \frac{\tilde{\rho}_m(t)}{V_m} \right] + \text{h.c.}$$

The integrals can be evaluated by introducing the Fourier modes of the operators

$$\tilde{S}_{mm'}^\alpha(t) = \sum_{\omega} e^{-i\omega t} \mathbf{L}_{mm'}^\alpha(\omega). \quad (58)$$

As we now show, the frequencies ω are related to the eigenfrequencies of H_m . Introducing the notation, $H_m |\lambda_m\rangle = \xi_{\lambda_m} |\lambda_m\rangle$ we write

$$R_m(t) = \sum_{\lambda} e^{it\xi_{\lambda_m}} |\lambda_m\rangle\langle\lambda_m|, \quad (59)$$

resulting in,

$$\tilde{S}_{mm'}^\alpha(t) = \sum_{\lambda, \nu} e^{it(\xi_{\lambda_m} - \xi_{\nu_{m'}})} F_{mm'}^{\alpha\lambda\nu} |\lambda_m\rangle\langle\nu_{m'}|, \quad (60)$$

where $F_{mm'}^{\alpha\lambda\nu} = \langle\lambda_m|S_\alpha|\nu_{m'}\rangle$ are complex scalars satisfying,

$$F_{mm'}^{\alpha\lambda\nu} = (F_{m'm}^{\alpha\nu\lambda})^*. \quad (61)$$

In general, the eigenvectors from different m 's are not orthogonal, i.e., $\langle\nu_{m'}|\lambda_m\rangle \neq \delta_{\lambda,\nu}$, for $m \neq m'$.

Equation (60) leads to the eigenfrequencies $\omega = \omega(\lambda_m, \nu_{m'}) = -\xi_{\lambda_m} + \xi_{\nu_{m'}}$, and the corresponding Fourier modes, $\mathbf{L}_{mm'}^\alpha(\omega) = F_{\lambda_m, \nu_{m'}}^\alpha |\lambda_m\rangle\langle\nu_{m'}|$. Here we consider the case of nondegenerate frequencies, i.e., if $\omega(\lambda_m, \nu_{m'}) = \omega(\lambda'_m, \nu'_{m'})$, then $\lambda_m = \lambda'_m$ and $\nu_{m'} = \nu'_{m'}$. To simplify the notation, we carry on the calculation with the summation over ω , keeping in mind the explicit dependence on the eigenvalues of H_m and $H_{m'}$. Using the Fourier decomposition we find,

$$\partial_t \tilde{\rho}_m = \sum_{m' \alpha \beta} \sum_{\omega, \omega'} e^{it(\omega' + \omega)} W_{mm'}^{\alpha\beta}(\omega) \left[\mathbf{L}_{mm'}^\alpha(\omega) \frac{\tilde{\rho}_{m'}}{V_{m'}} \mathbf{L}_{m'm}^\beta(\omega') - \mathbf{L}_{mm'}^\alpha(\omega) \mathbf{L}_{m'm}^\beta(\omega') \frac{\tilde{\rho}_m}{V_m} \right] + \text{h.c.}, \quad (62)$$

where we introduced,

$$W_{mm'}^{\alpha\beta}(\omega) = \int_0^\infty d\tau e^{-i\tau\omega} C_{mm'}^{\alpha\beta}(\tau). \quad (63)$$

Secular approximation.—We retain only terms with $\omega' = -\omega$. However, note that, since V is Hermitian,

$$\sum_{\alpha} S_\alpha \otimes B_\alpha = \sum_{\alpha} S_\alpha^\dagger \otimes B_\alpha^\dagger. \quad (64)$$

That is, either the terms in the sum are Hermitian or the sum contains their Hermitian conjugate. For simplicity, let us assume henceforth that at least the system operators are Hermitian, $S_\alpha = S_\alpha^\dagger$, $\forall \alpha$. This implies that,

$$\mathbf{L}_{m',m}^\alpha(-\omega) = [\mathbf{L}_{m,m'}^\alpha(\omega)]^\dagger = (F_{mm'}^{\alpha\lambda\nu})^* |\nu_{m'}\rangle\langle\lambda_m|. \quad (65)$$

Rotating back to the original frame, we find the general form of the MARE,

$$\partial_t \rho_m = -i[H_m + H_m^{\text{LS}}, \rho_m] + \sum_{m'} \sum_{\lambda\nu} \Gamma_{mm'}^{\lambda\nu} \left[|\lambda_m\rangle\langle\nu_{m'}| \frac{\rho_{m'}}{V_{m'}} |\nu_{m'}\rangle\langle\lambda_m| - \frac{1}{2} \left\{ |\lambda_m\rangle\langle\lambda_m|, \frac{\rho_m}{V_m} \right\} \right], \quad (66)$$

where

$$H_m^{\text{LS}} = - \sum_{m'} \sum_{\lambda\nu} \zeta_{mm'}^{\lambda\nu} |\lambda_m\rangle\langle\lambda_m|, \quad (67)$$

and

$$\sum_{\alpha\beta} W_{mm'}^{\alpha\beta} F_{mm'}^{\alpha\lambda\nu} \left(F_{mm'}^{\beta\lambda\nu} \right)^* =: \Gamma_{mm'}^{\lambda\nu} / 2 + i\zeta_{mm'}^{\lambda\nu}. \quad (68)$$

From the properties in Eq. (57, 61) the rates are symmetric tensors,

$$\Gamma_{mm'}^{\lambda\nu} = \Gamma_{m'm}^{\nu\lambda}, \quad (69)$$

which is understood as a generalized detailed balance condition. In general, the above MARE does not have a conserved quantity as Eq. (2). It has been shown in Ref. [36] that under very general conditions the generator of non-Markovian evolution can be written as Eq. (66), but previous microscopic derivations [38, 39] obtained a simpler structure. We have obtained the generator in its general form explicitly, i.e., with m -dependent jump operators.

A.2 Trace-preservation

The results from Ref. [36] assure that Eq. (66) generates a completely-positive and trace-preserving evolution (CPTP) of ρ_S . Yet, it is instructive to show trace-preservation. Introducing,

$$q(m, \lambda, \nu) = \langle \lambda_m | \rho_m | \nu_m \rangle = [q(m, \nu, \lambda)]^*, \quad \lambda \neq \nu, \quad (70)$$

$$p(m, \lambda) = \langle \lambda_m | \rho_m | \lambda_m \rangle, \quad (71)$$

we can decouple coherences from populations in Eq. (66),

$$\partial_t q(m, \lambda, \nu) = - \left[i(\bar{\xi}_{\lambda_m} - \bar{\xi}_{\nu_m}) + \sum_{m'\eta} \frac{\Gamma_{mm'}^{\lambda\eta} + \Gamma_{mm'}^{\nu\eta}}{2V_m} \right] q(m, \lambda, \nu) \quad (72)$$

$$\partial_t p(m, \lambda) = \sum_{m'} \sum_{\nu} \Gamma_{mm'}^{\lambda\nu} \left[\frac{p(m', \nu)}{V_{m'}} - \frac{p(m, \lambda)}{V_m} \right], \quad (73)$$

with $(H_m + H_m^{\text{LS}}) |\lambda_m\rangle = \bar{\xi}_{\lambda_m} |\lambda_m\rangle$. Trace preservation of the system density matrix is equivalent to $\sum_{\lambda m} \partial_t P(m, \lambda) = 0$. Performing the sum, we conclude that this is the case due to the detailed balance condition in Eq. (69).

B Inhomogeneous Anisotropic Central Spin Model

We now particularize the microscopic derivation of App. ?? to a Hamiltonian that is more general than Eq. (1) in the main text, including inhomogeneity in the anisotropy tensor. The interaction term can be written as,

$$H_{SB} = \sum_k \sum_{\alpha=x,y,z} \left[A_k^{\alpha,z} S_\alpha I_k^z + S_\alpha (A_k^{\alpha,+} I_k^+ + A_k^{\alpha,-} I_k^-) \right] = \sum_\alpha S_\alpha (\mathbf{B}_\alpha^z + \mathbf{B}_\alpha^+ + \mathbf{B}_\alpha^-)$$

where S_α are spin-1/2 operators, $A_k^{\alpha,\beta}$, $\alpha, \beta = x, y, z$ are elements of the inhomogeneous anisotropy tensor, \mathbf{A}_k , and we introduced $A_k^{\alpha,\pm} = A_k^{\alpha,x} \pm i A_k^{\alpha,y}$. In the second equality we introduced the operators,

$$\mathbf{B}_\alpha^l = \sum_k A_k^{\alpha,l} I_k^l. \quad (74)$$

We now split the interaction as in Eq. (47), by noting that

$$\langle H_{SB} \rangle_m = \sum_\alpha S_\alpha \langle \mathbf{B}_\alpha^z \rangle_m = m \sum_\alpha \bar{A}_{\alpha,z} S_\alpha, \quad (75)$$

with $\bar{A}_{\alpha,z} = \sum_k A_k^{\alpha,z}/N$. Thus

$$\delta H = \sum_{\alpha} \bar{A}_{\alpha,z} S_{\alpha} J_z, \quad V = \sum_{\alpha} S_{\alpha} (\delta B_{\alpha}^z + B_{\alpha}^+ + B_{\alpha}^-) = \sum_{\alpha} S_{\alpha} \otimes C_{\alpha}, \quad (76)$$

where $J_z = \sum_k I_k^z$,

$$\delta B_{\alpha}^z = \sum_k \delta A_k^{\alpha,z} I_k^z, \quad C_{\alpha} = \delta B_{\alpha}^z + B_{\alpha}^+ + B_{\alpha}^-, \quad (77)$$

and $\delta A_k^{\alpha,z} = A_k^{\alpha,z} - \bar{A}_{\alpha,z}$ quantifies the inhomogeneity. Note that V is now in the form required in the general derivation, Eq. (54), and the operators involved in the product structure are Hermitian, $S_{\alpha}^{\dagger} = S_{\alpha}$, $C_{\alpha}^{\dagger} = C_{\alpha}$. According to δH , the m -resolved Hamiltonian now reads,

$$H_m = \vec{B}_0 \cdot \vec{S} + m \sum_{\alpha} \bar{A}_{\alpha,z} S_{\alpha} = \vec{B}_m \cdot \vec{S}, \quad \vec{B}_m = \vec{B}_0 + m \sum_{\alpha} \bar{A}_{\alpha,z} \hat{e}_{\alpha}, \quad (78)$$

with eigenvalues $\pm \xi_m$ and eigenvectors $|\uparrow_m\rangle, |\downarrow_m\rangle$. From Eq. (49), we obtain the unitary transformation,

$$R(t) = e^{it \sum_k \omega_k I_k^z} R_m(t), \quad R_m(t) = e^{i\xi_m t} |\uparrow_m\rangle\langle\uparrow_m| + e^{-i\xi_m t} |\downarrow_m\rangle\langle\downarrow_m|. \quad (79)$$

All the steps of the general derivation now follow. We now seek to achieve the form presented in Eq. (2) by computing the correlation functions explicitly. We write,

$$C_{mm'}^{\alpha\beta}(\tau) = \text{tr} \left\{ \Pi_m \tilde{C}_{\alpha}(\tau) \Pi_{m'} C_{\beta} \right\} = \sum_{j=+, -, z} C_{mm'}^{\alpha\beta j}(\tau), \quad (80)$$

with,

$$C_{mm'}^{\alpha\beta, z}(\tau) = \text{tr} \left\{ \Pi_m \delta \tilde{B}_{\alpha}^z(\tau) \Pi_{m'} \delta B_{\beta}^z \right\}, \quad (81)$$

$$C_{mm'}^{\alpha\beta, +}(\tau) = \text{tr} \left\{ \Pi_m \tilde{B}_{\alpha}^+(\tau) \Pi_{m'} B_{\beta}^- \right\}, \quad (82)$$

$$C_{mm'}^{\alpha\beta, -}(\tau) = \text{tr} \left\{ \Pi_m \tilde{B}_{\alpha}^-(\tau) \Pi_{m'} B_{\beta}^- \right\}. \quad (83)$$

We start by discussing Eq. (81) which entails processes induced purely by the inhomogeneity. Since $[\delta B_{\alpha}^z, I_k^z] = 0$, this correlation function is proportional to $\delta_{mm'}$ and is time-independent, $\delta \tilde{B}_{\alpha}^z(\tau) = \delta B_{\alpha}^z$. The former means that no jumps in the bath are induced and the latter that the correlation function does not decay, violating the Markov approximation.

We now focus on a spin-1/2 environment, see App. B.1 for approximations for arbitrary spin. We find

$$C_{mm'}^{\alpha\beta, z}(\tau) = \delta_{m,m'} \sum_k \delta A_k^{\alpha,z} \delta A_k^{\beta,z} V_m \frac{N^2 - 4m^2}{4N(N-1)}, \quad (84)$$

where the volume factors denote the number of states with total magnetization m [59, 82] and are given by

$$V_m = \frac{N!}{(N/2 + m)!(N/2 - m)!}. \quad (85)$$

The time independence in Eq. (84) is a consequence of the fact that our Hamiltonian in Eq. (1) does not include any T_1 processes on the bath (e.g. spin-flips/thermalization). In reality, the correlation function in Eq. (81) decays with the T_1 time of the bath (see, for instance Ref. [22]). We thus treat this correlation function phenomenologically as

$$C_{mm'}^{\alpha\beta, z}(\tau) = \delta_{m,m'} e^{-|\tau|/T_1} C_{mm'}^{\alpha\beta, z}(0), \quad (86)$$

where $C_{mm'}^{\alpha,z}(0)$ is given by Eq. (84).

We now concentrate on evaluating Eq. (82). Writing out,

$$C_{mm'}^{\alpha\beta,+}(-\tau) = \sum_k A_k^{\alpha,+} A_k^{\beta,-} e^{-i\tau\omega_k} r_{mm'}^+, \quad r_{mm'}^+ = \text{tr}\{\Pi_m I_k^+ \Pi_{m'} I_k^-\}, \quad (87)$$

we find

$$r_{mm'}^+ = \delta_{m',m-1} \text{tr}\{\Pi_m I_k^+ I_k^-\} = V_m \delta_{m',m-1} \left(\frac{1}{2} + \frac{m}{N} \right). \quad (88)$$

The correlation function then reads,

$$C_{mm'}^{\alpha\beta,+}(\tau) = \delta_{m',m-1} V_m \frac{N/2 + m}{N} \int_{-\infty}^{\infty} d\omega \varrho_{\alpha\beta}(\omega) e^{i\tau\omega}.$$

In the last equality we introduced the spectral densities [83]

$$\varrho_{\alpha\beta}(\omega) = \sum_{k=1}^N A_k^{\alpha,+} A_k^{\beta,-} \delta(\omega - \omega_k). \quad (89)$$

Similarly, we find,

$$C_{mm'}^{\alpha\beta,-} = \delta_{m',m+1} V_m \frac{N/2 - m}{N} \int_{-\infty}^{\infty} d\omega \varrho_{\alpha\beta}(\omega) e^{-i\tau\omega}. \quad (90)$$

We now determine the jump operators featuring in the MARE. Equation (79) fully determines the Fourier components,

$$\tilde{S}_{mm'}^\alpha(t) = R_m(t) S_\alpha R_{m'}^\dagger(t) = \sum_\omega e^{-i\omega t} L_{mm'}^\alpha(\omega), \quad (91)$$

where

$$L_{mm'}^\alpha(\xi_m + \xi_{m'}) = F_{mm'}^{\alpha,\downarrow,\uparrow} |\downarrow_m\rangle \langle \uparrow_{m'}|, \quad (92)$$

$$L_{mm'}^\alpha(-\xi_m - \xi_{m'}) = F_{mm'}^{\alpha,\uparrow,\downarrow} |\uparrow_m\rangle \langle \downarrow_{m'}|, \quad (93)$$

$$L_{mm'}^\alpha(\xi_m - \xi_{m'}) = F_{mm'}^{\alpha,\downarrow,\downarrow} |\downarrow_m\rangle \langle \downarrow_{m'}|, \quad (94)$$

$$L_{mm'}^\alpha(-\xi_m + \xi_{m'}) = F_{mm'}^{\alpha,\uparrow,\uparrow} |\uparrow_m\rangle \langle \uparrow_{m'}|, \quad (95)$$

and we used the notation $F_{mm'}^{\alpha,\lambda,\nu} = \langle \lambda_m | S_\alpha | \nu_{m'} \rangle$. Crucially, the above establish the set of eigenfrequencies,

$$\{\xi_m + \xi_{m'}, -\xi_m - \xi_{m'}, \xi_m - \xi_{m'}, -\xi_m + \xi_{m'}\}, \quad (96)$$

with $\xi_m \geq 0$. From Eq. (63), we find

$$W_{mm}^{\alpha\beta}(\omega) = T_1 \frac{1 - i\omega T_1}{1 + (\omega T_1)^2} \sum_k \delta A_k^{\alpha,z} \delta A_k^{\beta,z} \frac{V_m}{4} \frac{2Nm^2 - 1}{N - 1}, \quad (97)$$

as well as

$$W_{mm-1}^{\alpha\beta}(\omega) = V_m \frac{N/2 + m}{N} \left[\pi \varrho_{\alpha\beta}(\omega) - i \text{p.v.} \int d\nu \frac{\varrho_{\alpha\beta}(\nu)}{\omega - \nu} \right], \quad (98)$$

and

$$W_{mm+1}^{\alpha\beta}(\omega) = V_m \frac{N/2 - m}{N} \left[\pi \varrho_{\alpha\beta}(-\omega) + i \text{p.v.} \int d\nu \frac{\varrho_{\alpha\beta}(\nu)}{\omega + \nu} \right], \quad (99)$$

where p.v. indicates the Cauchy principal value. The real parts of these quantities determine the rates in the MARE while the imaginary parts contribute to the Lamb shift, see Eq. (68). We may further

simplify the MARE by considering spectral densities that vanish at low (and negative) frequencies, such that

$$\varrho_{\alpha\beta}(-\xi_m - \xi_{m'}) = \varrho_{\alpha\beta}[\pm(\xi_m - \xi_{m'})] = 0. \quad (100)$$

Furthermore, we assume that the splitting of the eigenenergies of H_m is large compared to the inverse T_1 time of the bath, such that

$$\frac{1}{1 + (\xi_m + \xi_{m'})^2 T_1^2} \simeq 0. \quad (101)$$

With these simplifications, we obtain the MARE

$$\begin{aligned} \partial_t \rho_m = & -i [\vec{B}_m \cdot \vec{S} + H_m^{\text{LS}}, \rho_m] + \gamma_m (\mathcal{D}[|\uparrow_m\rangle\langle\uparrow_m|] + \mathcal{D}[|\downarrow_m\rangle\langle\downarrow_m|]) \frac{\rho_m}{V_m} \\ & + \Gamma_m \left[|\downarrow_m\rangle\langle\uparrow_{m-1}| \frac{\rho_{m-1}}{V_{m-1}} |\uparrow_{m-1}\rangle\langle\downarrow_m| - \frac{1}{2} \left\{ |\downarrow_m\rangle\langle\downarrow_m|, \frac{\rho_m}{V_m} \right\} \right] \\ & + \Gamma_{m+1} \left[|\uparrow_m\rangle\langle\downarrow_{m+1}| \frac{\rho_{m+1}}{V_{m+1}} |\downarrow_{m+1}\rangle\langle\uparrow_m| - \frac{1}{2} \left\{ |\uparrow_m\rangle\langle\uparrow_m|, \frac{\rho_m}{V_m} \right\} \right], \end{aligned} \quad (102)$$

with the rates

$$\Gamma_m = 2\pi V_m \left(\frac{1}{2} + \frac{m}{N} \right) \sum_{\alpha\beta} \text{Re} \left\{ \varrho_{\alpha\beta}(\xi_m + \xi_{m-1}) F_{m,m-1}^{\alpha\downarrow\uparrow} (F_{m,m-1}^{\beta\uparrow\downarrow})^* \right\}, \quad (103)$$

$$\gamma_m = T_1 \sum_k \sum_{\alpha\beta} \delta A_k^{\alpha,z} \delta A_k^{\beta,z} V_m \frac{N^2 - 4m^2}{4N(N-1)}, \quad (104)$$

and the Lamb shift can be computed from Eqs. (67) and (68). To arrive at Eq. (2) in the main text, we drop the Lamb-shift Hamiltonian, and we set $\gamma_m = 0$ by neglecting the k -dependence in the system-bath coupling.

B.1 Large spin- s bath

We consider a bath with $N \gg 1$ identical spins and each spin has spin s . Counting the possible states whose azimuthal projection add up to a given value m becomes impossible. However, an approximate value can be given in the large N -limit, due to the central limit theorem. To this end, we use a probabilistic approach: we consider the infinite temperature state, where each micro-state is equally likely. We then consider the probability, p_m , that we find a given magnetization, m . The volume factor then reads

$$V_m = (2s + 1)^N p_m, \quad (105)$$

where $(2s + 1)^N$ is total number of possible configurations. In the infinite temperature state, the average and variance of a single spin are given by,

$$\mu = \langle S_z \rangle = \frac{1}{2s + 1} \sum_{j=-s}^s j = 0, \quad \varsigma_s^2 = \text{var}(S_z) = \frac{1}{2s + 1} \sum_{j=-s}^s j^2 = \frac{s(s + 1)}{3}. \quad (106)$$

For non-interacting spins, the total magnetization satisfies a central-limit theorem and we have

$$p_m(s) \approx \frac{3}{\sqrt{2\pi N \varsigma_s}} e^{-\frac{m^2}{N \varsigma_s^2}} \quad (107)$$

which fully determines the volumes. This problem is equivalent to computing the microcanonical partition function of a Boltzmann gas [58].

As a consequence, the spectral properties of a large ensemble of N spin- s nuclei can be emulated by a larger ensemble of N' spin-1/2 nuclei, as long as both produce the same distribution. Since Eq. (107) is fully determined by its variance, the condition is,

$$N' = \frac{4}{3}Ns(s+1). \quad (108)$$

Thus, using this relation we can use all the results for spin-1/2 replacing N by N' . In particular,

$$V_m \approx \frac{[4/3Ns(s+1)]!}{[2/3Ns(s+1) + m]![2/3Ns(s+1) - m]!}. \quad (109)$$

We now compute the rate in Eq. (88). The calculation is possible by rewriting it fully in terms of the above volume factors, and thus holds under the large N limit. To achieve this, we first, note that since Eq. (88) has permutation invariance with respect to k , we can sum over k and divide by N without changing the result,

$$\text{tr}\{\Pi_m I_k^\dagger I_k\} = \frac{1}{N} \text{tr}\{\Pi_m J^+ J\}, \quad (110)$$

where $J = \sum_k I_k$ are total spin operators. We now proceed by performing the calculation in the Dicke basis, in which the projectors write,

$$\Pi_m = \sum_{j=|m|}^{sN} \sum_{d=1}^{d_j} |jmd\rangle\langle jmd|, \quad (111)$$

where $\vec{J} \cdot \vec{J} |jmd\rangle = j(j+1) |jmd\rangle$, and d are degeneracies of each Dicke state due to permutations with the same j, m . Using standard relations from angular momenta,

$$\text{tr}\{\Pi_m J^\dagger J\} = \sum_{j'=|m|}^{sN} d_j [j(j+1) - m(m-1)]. \quad (112)$$

The degeneracies of the Dicke states satisfy the property,

$$\sum_{j=|m|}^{sN} d_j = V_m. \quad (113)$$

For a detailed discussion on the degeneracy of Dicke states, see Ref. [82]. This allows the second term in the square brackets above to be summed directly, and implies that $d_j = V_j - V_{j+1}$. We thus have,

$$\text{tr}\{\Pi_m J^\dagger J\} = V_m \sum_{j=|m|}^{sN} (V_j - V_{j+1}) [j(j+1) - m(m-1)] \quad (114)$$

So far, we have not performed any approximation, and the steps do not depend on the value of s . The calculation is finished by using the approximate expression for the the volumes, Eq. (109), and we have,

$$V_j - V_{j+1} = \frac{(2j+1)N'!}{(N'/2 + j + 1)!(N'/2 - j)!}, \quad j \leq \frac{N'}{2}. \quad (115)$$

With the above expression we can perform the sum in Eq. (114). As expected, the result is the same as for $s = 1/2$, but with $N \rightarrow N' = N(4s/3)(s+1)$,

$$r_{mm'}^+(s) = \delta_{m',m-1} V_m \left[\frac{2}{3}s(s+1) + \frac{m}{N} \right], \quad (116)$$

resulting in the rates

$$\Gamma_m = 2\pi V_m \left[\frac{2}{3}s(s+1) + \frac{m}{N} \right] \sum_{\alpha\beta} \text{Re}\left\{ \varrho_{\alpha\beta}(\xi_m + \xi_{m-1}) F_{m,m-1}^{\alpha\downarrow\uparrow} \left(F_{m,m-1}^{\beta\downarrow\uparrow} \right)^* \right\}. \quad (117)$$

The same rates have been found in Ref. [57] via a heuristic argument.

B.2 Conserved quantity

We now show that Eq. (2) conserves the quantity,

$$M = m + \hat{B}_m \cdot \vec{S}. \quad (118)$$

Note that even the average of this quantity, $\langle M \rangle$, in general contains correlations between system and bath, since $\hat{B}_m \cdot \vec{S}$ is an m -dependent operator. To show the conservation law, we observe that

$$\hat{B}_m \cdot \vec{S} |\uparrow_m / \downarrow_m\rangle = \pm \frac{1}{2} |\uparrow_m / \downarrow_m\rangle, \quad \forall m, \quad (119)$$

i.e., the eigenvalues do not depend on m . With this observation, we can follow a similar argument to Ref. [38]: we show that the equation for the populations, $\partial_t p(\uparrow / \downarrow, m)$, implies that $\partial_t P(M) = 0$, with

$$P(M) = \sum_m \sum_{\sigma=\pm 1/2} \delta_{M, m+\sigma} p(\sigma, m), \quad (120)$$

where $p(1/2, m) = p(\uparrow, m)$ and $p(-1/2, m) = p(\downarrow, m)$. Using Eqs. (4) and (5), we find

$$\begin{aligned} \partial_t P(M) = & \Gamma_{M-1/2} \frac{p(\uparrow, M-1/2)}{V_{M-1/2}} - \Gamma_{M+1/2} \frac{p(\downarrow, M+1/2)}{V_{M-1/2}} \\ & + \Gamma_{M+1/2} \frac{p(\downarrow, M+1/2)}{V_{M-1/2}} - \Gamma_{M-1/2} \frac{p(\uparrow, M-1/2)}{V_{M-1/2}} = 0. \end{aligned} \quad (121)$$

B.3 Analytic solution

We follow Ref. [38] and use the conserved quantity to construct the propagator acting on the populations, Eqs. (4, 5). The evolution of the coherent part is simple and does not couple to the populations—we leave it for last. We emphasize that the equations of populations and coherences in general only decouple in the m -dependent basis spanned by $\{|\sigma_m\rangle\}_{\sigma,m}$. The conservation of M implies that the jump processes allowed by the MARE must conserve M , implying that the propagator can be decomposed as

$$K = \bigoplus_M K_{|M}, \quad (122)$$

where $K_{|M}$ is the restriction of K to the subspace with a fixed M ; these are two-dimensional subspaces spanned by pairs of the form, $p(\uparrow, m)$, $p(\downarrow, m+1)$. To make progress, we introduce the vector,

$$\vec{p} = \begin{pmatrix} \vdots \\ p(\uparrow, m-1) \\ p(\downarrow, m) \\ p(\uparrow, m) \\ p(\downarrow, m+1) \\ \vdots \end{pmatrix}, \quad (123)$$

and write Eqs. (4, 5) as $\partial_t \vec{p} = G \vec{p}$, where $G = \bigoplus_M G_{|M}$ with

$$G_{|M} = \frac{\Gamma_{m+1}}{V_m} \begin{pmatrix} -1 & \frac{V_m}{V_{m+1}} \\ 1 & -\frac{V_m}{V_{m+1}} \end{pmatrix}. \quad (124)$$

Then, we simply have to exponentiate each block

$$K_{|M} = e^{tG_{|M}} = \mathbb{1}_{|M} + \frac{1 - e^{-t\bar{\Gamma}_m}}{\bar{\Gamma}_m} G_{|M} = \mathbb{1}_{|M} + \frac{1 - e^{-t\bar{\Gamma}_m}}{1 + V_m/V_{m+1}} \begin{pmatrix} -1 & \frac{V_m}{V_{m+1}} \\ 1 & -\frac{V_m}{V_{m+1}} \end{pmatrix},$$

where we introduced,

$$\bar{\Gamma}_m = \frac{\Gamma_{m+1}}{V_m} \left(1 + \frac{V_m}{V_{m+1}} \right). \quad (125)$$

In the long-time limit, this propagator implies that the populations in the m -dependent basis must satisfy

$$\frac{p_{\text{ss}}(\downarrow, m+1)}{p_{\text{ss}}(\uparrow, m)} = \frac{V_{m+1}}{V_m}. \quad (126)$$

We now discuss the coherent sector; $q(\sigma, \nu, m) = \langle \sigma_m | \rho_m | \nu_m \rangle$. From the MARE (102),

$$\partial_t q(\sigma, \nu, m) = - \left[2i\xi_m + \frac{\gamma_m + \Gamma_m + \Gamma_{m+1}}{2V_m} \right] q(\sigma, \nu, m). \quad (127)$$

The above equation can be directly exponentiated, and we are done constructing the analytic solution. The plots in the main text are obtained by implementing the solutions numerically and evolving initial conditions. For the spin qubit, we use a cutoff for $|m|$ equal to $N/50$. This is justified since P_m is never polarized excessively and leads to errors of the order of 10^{-10} .

B.4 Second law of thermodynamics

The existence of a conserved quantity also allows us to generalize the second law of thermodynamics from Ref. [38] to the MARE. We consider the observational entropy

$$S_{\text{obs}} = \sum_{\sigma, m} p(\sigma, m) [-\ln p(\sigma, m) + \ln V_m]. \quad (128)$$

In this appendix, we prove that

$$\partial_t S_{\text{obs}} \geq 0. \quad (129)$$

The crucial step is to show that the above is minus the time-derivative of the Kullback-Leibler divergence between the generic probability vector \vec{p} and the corresponding steady-state vector, \vec{p}_{ss} ;

$$\partial_t D_{\text{KL}}(\vec{p} \mid \vec{p}_{\text{ss}}) = \partial_t \sum_{\sigma m} p(\sigma, m) \ln \frac{p(\sigma, m)}{p_{\text{ss}}(\sigma, m)}. \quad (130)$$

It suffices to concentrate on,

$$\begin{aligned} \partial_t \sum_{\sigma, m} p(\sigma, m) \ln p_{\text{ss}}(\sigma, m) &= \partial_t \sum_m p(\uparrow, m) \ln p_{\text{ss}}(\uparrow, m) + p(\downarrow, m) \ln p_{\text{ss}}(\downarrow, m) \\ &= \partial_t \sum_m [P(M = m + 1/2) - p(\downarrow, m + 1)] \ln p_{\text{ss}}(\uparrow, m) + p(\downarrow, m) \ln p_{\text{ss}}(\downarrow, m) \\ &= \partial_t \sum_m p(\downarrow, m) \ln p_{\text{ss}}(\downarrow, m) - p(\downarrow, m + 1) \ln p_{\text{ss}}(\uparrow, m), \end{aligned} \quad (131)$$

where we used that $P(M) = \sum_{\sigma, m} \delta_{M, m+\sigma} p(\sigma, m)$, $\partial_t P(M) = 0$, $\partial_t p_{\text{ss}}(\sigma, m) = 0$. We now use Eq. (126)

$$\begin{aligned} \partial_t \sum_{\sigma, m} p(\sigma, m) \ln p_{\text{ss}}(\sigma, m) &= \partial_t \sum_m p(\downarrow, m) \ln p_{\text{ss}}(\downarrow, m) \\ &\quad - \partial_t \sum_m p(\downarrow, m + 1) \ln p_{\text{ss}}(\downarrow, m + 1) - \partial_t \sum_m p(\downarrow, m + 1) \ln \frac{V_{m+1}}{V_m}. \end{aligned} \quad (132)$$

The first two terms cancel each other upon change of indices and we are left with,

$$\begin{aligned} -\partial_t \sum_{\sigma, m} p(\sigma, m) \ln p_{\text{ss}}(\sigma, m) &= -\partial_t \sum_m [p(\downarrow, m+1) \ln V_{m+1} - p(\downarrow, m+1) \ln V_m] \\ &= -\partial_t \sum_m [p(\downarrow, m) \ln V_m + p(\uparrow, m) \ln V_m] = -\partial_t \sum_{\sigma, m} p(\sigma, m) \ln V_m, \end{aligned} \quad (133)$$

where we used again the definition of $P(M)$ and the conservation law, $\partial_t P(M) = 0$. With the result above, we have that

$$\partial_t D_{\text{KL}}(\vec{p}|\vec{p}_{\text{ss}}) = -\partial_t S_{\text{obs}} \quad (134)$$

To complete the proof, we note that the dynamics of \vec{p} is Markovian, see Eqs. (4, 5). Then, we can use the data-processing inequality [84], which implies

$$-\partial_t D_{\text{KL}}(\vec{p}|\vec{p}_{\text{ss}}) \geq 0, \quad (135)$$

and we have shown that Eq. (129) is satisfied.

B.5 Decomposing the observational entropy

Here we consider decompositions of the observational entropy. To this end, we note that it can be split in terms of marginal entropies and coarse-grained mutual information [38],

$$\mathcal{S}_{\text{obs}} = \mathcal{S}_B(P) + \mathcal{S}(p_S) - D_{\text{KL}}[\vec{p}|P \ p_S] + \sum_m P_m \ln V_m. \quad (136)$$

We further note that $\mathcal{S}(p_S)$ —the Shannon entropy of the marginal $p_S(\sigma) = \sum_m p(\sigma, m)$ —does not bear an obvious relation with the von Neumann entropy of the system. It can however be associated to the von Neumann entropy of a generalized dephasing map, \mathcal{D} , acting on ρ_S ,

$$\mathcal{D}\rho_S = \sum_m \mathcal{D}_m(\rho_m) = \sum_m \frac{1}{2\pi} \int_0^{2\pi} d\chi e^{i\chi \hat{B}_m \cdot \vec{S}} \rho_m e^{-i\chi \hat{B}_m \cdot \vec{S}}. \quad (137)$$

We then write,

$$\mathcal{S}(p_S) = S(\rho_S) + \mathcal{C}_{\text{rel}}, \quad (138)$$

where we introduced the (generalized) relative entropy of coherence [85],

$$\mathcal{C}_{\text{rel}} = \mathcal{S}(\mathcal{D}\rho_S) - \mathcal{S}(\rho_S). \quad (139)$$

We can then write the observational entropy as,

$$\mathcal{S}_{\text{obs}} = \mathcal{S}_B(P) + \mathcal{S}(\rho_S) + \mathcal{C}_{\text{rel}} - D_{\text{KL}}[\vec{p}|P \ p_S] + \sum_m P_m \ln V_m. \quad (140)$$

Finally, we argue that $\mathcal{C}_{\text{rel}} \geq 0$. Note that \mathcal{D} is CPTP and unital, $\mathcal{D}(\mathbb{1}) = \mathbb{1}$. Using the monotonicity of the quantum relative entropy under CPTP maps [86],

$$D_{\text{KL}}(\rho_S|\mathbb{1}) \geq D_{\text{KL}}[\mathcal{D}(\rho_S)|\mathcal{D}(\mathbb{1})], \quad \Rightarrow \quad \mathcal{S}(\mathcal{D}\rho_S) \geq \mathcal{S}(\rho_S), \quad (141)$$

Therefore, $\mathcal{C}_{\text{rel}} \geq 0$. That is, the von Neumann entropy of the system discussed in the main text lower bounds the entropy of the marginal,

$$\mathcal{S}(\mathcal{D}\rho_S) \geq \mathcal{S}(\rho_S). \quad (142)$$

C Superconducting qubit

Below we derive Eq. (13) by providing an effective Hamiltonian and specializing the results of App. B.

C.1 Schrieffer-Wolff transformation

In this subsection we consider TLSs with arbitrary frequencies. Via Schrieffer-Wolff perturbation theory we show that the far off-resonant TLSs do not contribute to the magnetization exchange processes and justify concentrating on the quasi-resonant TLSs. We consider the Hamiltonian $H = H_0 + V$ with

$$H_0 = \omega_S S_z + \sum_{k=1}^{N_{\text{tot}}} \omega_k S_z^k, \quad (143)$$

and the coupling Hamiltonian

$$V = \sum_{k=1}^{N_{\text{tot}}} A_k \vec{S} \cdot \vec{S}_k = \sum_{k=1}^{N_{\text{tot}}} A_k S_z S_z^k + \frac{1}{2} \sum_{k=1}^{N_{\text{tot}}} A_k (S^\dagger S_k + S_k^\dagger S), \quad (144)$$

with $\vec{S}_{(k)} = (S_x^{(k)}, S_y^{(k)}, S_z^{(k)})$. We consider cases in which V represents *weak* coupling, with hyperfine constants A_k . The TLSs ensemble can be decomposed into two parts: the quasi-resonant TLSs that have a frequency close to ω_S and the TLSs that are off-resonant. The set of quasi-resonant TLSs is defined by

$$O_\delta = \{\omega_k : |\omega_k - \omega_S| < \delta\}. \quad (145)$$

The off-resonant TLSs have frequencies $\omega_k \notin O_\delta$ that are farther than δ away from ω_S . Following Ref. [87], we may then apply a Schrieffer-Wolff transformation to reduce the interaction to

$$V \approx \sum_{k:\omega_k \in O_\delta} A_k \vec{S} \cdot \vec{S}_k + \sum_{k:\omega_k \notin O_\delta} \frac{A_k^2}{\Delta_k} S_z^k S_z, \quad (146)$$

where $\Delta_k = \omega_k - \omega_S$. Assuming the off-resonant TLS to be in a state that is diagonal in the basis of S_z^k , their effect on the system is fully captured by a random but time-independent shift in the frequency ω_S . Since we do not investigate the coherence properties of the superconducting qubit, this has no effect on our results and we drop it in the following.

C.2 MARE for the superconducting qubit

We start by writing the Hamiltonian obtained from the Schrieffer-Wolff perturbation theory as,

$$H = H_S + \delta H + H_B + V, \quad (147)$$

$$H_S = \omega_S S_z, \quad \delta H = a J_z, \quad V = \sum_{k=1}^N \delta A_k S_z S_z^k + \sum_{k=1}^N A_k (S_x S_k^x + S_y S_k^y), \quad (148)$$

where we introduced $a = \sum_{k=1}^N A_k / N$, $\delta A_k = A_k - Na$. Here, all A_k are perturbative and the sum runs only over quasi-resonant TLSs. The term associated to δA_k is small even compared with A_k , since we consider only quasi-resonant TLSs. This justifies discarding its contributions to the MARE. Thereby, the m -dependent Hamiltonian is simply,

$$H_m = \vec{B}_m \cdot \vec{S} = (\omega_S + am) S_z. \quad (149)$$

This Hamiltonian always leads to jumps between S_z eigenstates, and the jump operators will not depend on m and the MARE has the form,

$$\partial_t \rho_m = -i[\vec{B}_m \cdot \vec{S}, \rho_m] + \Gamma_m \left[\sigma \frac{\rho_{m-1}}{V_{m-1}} \sigma^\dagger - \frac{1}{2} \left\{ \sigma \sigma^\dagger, \frac{\rho_m}{V_m} \right\} \right] + \Gamma_{m+1} \left[\sigma^\dagger \frac{\rho_{m+1}}{V_{m+1}} \sigma - \frac{1}{2} \left\{ \sigma^\dagger \sigma, \frac{\rho_m}{V_m} \right\} \right],$$

where $\vec{B}_m = (\omega_S + Am)\hat{e}_z$. Above, the rates are given by,

$$\Gamma_m = V_m \left(\frac{1}{2} + \frac{m}{N} \right) \kappa_m, \quad (150)$$

with $\kappa_m = 2\pi\varrho(\omega_S + am)$. Reminding that A_k are perturbative and $a = \sum_k A_k/N$, we can approximate for the quasi-resonant TLSs $\varrho(\omega_S + am) \approx \varrho(\omega_S)$. The couplings κ_m then become independent of m and we recover Eq. (13). In general, for the quasi-resonant TLSs, the non-perturbative contribution is small and can be discarded, as long as $|Na| \ll \omega_S$. If the off-resonant TLSs are also included, or the region of quasi-resonant TLSs is very dense, this approximation is inadequate.

D Spin qubit

D.1 MARE for the spin qubit

For the spin qubit, we start from the Hamiltonian in Eq. (32). From Eq. (78), we obtain the m -resolved Hamiltonian,

$$H_m = \vec{B}_m \cdot \vec{S}, \quad \vec{B}_m = (\Delta + A_c m)\hat{e}_z + \Omega\hat{e}_x. \quad (151)$$

This Hamiltonian has the eigenstates

$$|\lambda_m\rangle = \sin(\chi_m^\lambda) |\downarrow_z\rangle + \cos(\chi_m^\lambda) |\uparrow_z\rangle, \quad \lambda = \downarrow, \uparrow \quad (152)$$

$$\chi_m^{\uparrow(\downarrow)} = \tan^{-1} \frac{\xi_m \pm \Delta_m}{\Omega}, \quad \xi_m = \frac{|\vec{B}_m|}{2} = \frac{1}{2} \sqrt{\Delta_m^2 + \Omega^2}, \quad (153)$$

where we used the shorthand, $\Delta_m = \Delta + A_c m$. To find the rates, we also need

$$|F_{mm'}^{\downarrow\uparrow}|^2 = |\langle \downarrow_m | S_z | \uparrow_{m'} \rangle|^2 = \frac{[(2\xi_m - \Delta_m)(2\xi_{m'} + \Delta_{m'}) + \Omega^2]^2}{64\xi_m\xi_{m'}(2\xi_m - \Delta_m)(2\xi_{m'} + \Delta_{m'})}. \quad (154)$$

The rates in the final MARE are then given by, see Eq. (117),

$$\Gamma_m = 2\pi V_m \left[\frac{2}{3}s(s+1) + \frac{m}{N} \right] |F_{m,m-1}^{\downarrow\uparrow}|^2 \varrho(\xi_m + \xi_{m\mp 1}). \quad (155)$$

We assume that the spectral density is Lorentzian, motivated by an exponential decay of the correlation functions at high Zeeman field [27, 32, 69],

$$\varrho(\omega) = 4A_{\text{nc}}^2 \frac{\gamma}{(\omega_B - \omega)^2 + \gamma^2}. \quad (156)$$

We observe that this form of the spectral density is a simplification. In spin qubits, the dominant nuclear dephasing leading to the decay of the bath correlation functions can be an electron(qubit)-mediated effect which demands the inclusion of higher order contributions of inhomogeneous flip-flop processes [32, 62, 69, 77] and strain-mediated quadrupole processes [26, 46]. Further, note that multiple nuclear species with different spins can be included by modifying the rates and including multiple peaks in the spectral densities at different species' characteristic frequencies. Below, we discuss the regime of validity of our approximations for typical experimental parameters.

D.2 Validity of the approximations

The Markov approximation is justified whenever the relaxation time of ρ_m , τ_m is small compared to the bath correlation time, $\tau_B = 1/\gamma$. In practice, the relaxation times τ_m can be estimated by,

$$\tau_m = \frac{1}{\Gamma_m} \leq \tau_R = \frac{1}{\Gamma_0}. \quad (157)$$

To obtain a conservative estimate, we assume Hartmann-Hahn resonance, $\Omega = \omega_B$ and $\tau_R \approx \gamma/(NA_{\text{nc}}^2)$. Thus, the condition for the Markov approximation is,

$$\frac{NA_{\text{nc}}^2}{\gamma^2} < 1. \quad (158)$$

The condition is satisfied for the parameters in Table 1.

The secular approximation discards terms in which the jump terms contain frequencies $\omega \neq \omega'$. The condition for the secular approximation is that oscillations with (difference) frequencies $|\omega - \omega'|$ are fast compared to the system relaxation time; i.e., $|\omega - \omega'|^{-1} \ll \tau_R$. As long as the spectral density is suppressed at frequencies close to zero (i.e., for the frequencies $|\xi_m - \xi_{m'}|$, only the frequencies $\omega = \xi_m + \xi_{m'}$ and $\omega' = -\xi_m - \xi_{m'}$ are relevant (see Eq. (96)). We have at Hartmann-Hahn resonance, $|\omega - \omega'| \geq 4 \min\{\xi_m, \xi_{m'}\} \geq 4\Omega$. A conservative estimate for the validity of the secular approximation is then,

$$\frac{A_{\text{nc}}^2 N}{4\gamma\Omega} < 1. \quad (159)$$

For the parameters in Table 1, the inequality is satisfied.